International Scientific-Technical and Production Journal

The Paton WELDING JOURNAL

July
2004
7

English translation of the monthly «Avtomaticheskaya Svarka» (Automatic Welding) journal published in Russian since 1948

Founders: *E.O. Paton Electric Welding Institute of the NAS of Ukraine*
International Association «Welding»

Publisher: *International Association «Welding»*

Editor-in-Chief B.E.Paton

Editorial board:

Yu.S.Borisov V.F.Grabin
Yu.Ya.Gretskii A.Ya.Ishchenko
B.V.Khitrovskaya V.F.Khorunov
I.V.Krivtsun
S.I.Kuchuk-Yatsenko
Yu.N.Lankin V.K.Lebedev
V.N.Lipodaev L.M.Lobanov
V.I.Makhnenko A.A.Mazur
V.F.Moshkin O.K.Nazarenko
I.K.Pokhodnya I.A.Ryabtsev
Yu.A.Sterenbogen N.M.Voropai
K.A.Yushchenko V.N.Zamkov
A.T.Zelnichenko

International editorial council:

N.P.Alyoshin (Russia)
B.Braithwaite (UK)
C.Boucher (France)
Guan Qiao (China)
U.Diltey (Germany)
P.Seyffarth (Germany)
A.S.Zubchenko (Russia)
T.Eagar (USA)
K.Inoue (Japan)
N.I.Nikiforov (Russia)
B.E.Paton (Ukraine)
Ya.Pilarczyk (Poland)
D. von Hofe (Germany)
Zhang Yanmin (China)
V.K.Sheleg (Belarus)

Promotion group:

V.N.Lipodaev, V.I.Lokteva
A.T.Zelnichenko (exec. director)
Translators:
S.A.Fomina, I.N.Kutianova,
T.K.Vasilenko
Editor
N.A.Dmitrieva
Electron galley:
I.S.Batasheva, T.Yu.Snegiryova

Address:
E.O. Paton Electric Welding Institute,
International Association «Welding»,
11, Bozhenko str., 03680, Kyiv, Ukraine
Tel.: (38044) 227 67 57
Fax: (38044) 268 04 86
E-mail: journal@paton.kiev.ua
http://www.nas.gov.ua/pwj

State Registration Certificate
KV 4790 of 09.01.2001

Subscriptions:
$460, 12 issues per year,
postage and packaging included.
Back issues available.

All rights reserved.
This publication and each of the articles contained herein are protected by copyright. Permission to reproduce material contained in this journal must be obtained in writing from the Publisher.
Copies of individual articles may be obtained from the Publisher.

CONTENTS

SCIENTIFIC AND TECHNICAL

Makhnenko V.I., Gajvoronsky A.A., Sarzhevsky V.A., Velikoivanenko E.A., Rozynka G.F. and **Pivtorak N.I.** Stresses in surfacing of parts made from high-carbon steels of the 65G type and risk of cold cracking 2

Maksimov S.Yu. and **Gurzhy A.A.** Modeling the conditions of pore initiation in the weld metal in wet underwater welding 7

Yushchenko K.A., Savchenko V.S. and **Zvyagintseva A.V.** Effect of heat treatment and degree of alloying on structural changes in nickel alloys 12

Grabin V.F., Golovko V.V., Kostin V.A. and **Alekseenko I.I.** Morphological peculiarities of microstructure of weld metal from low-alloy steels with ultralow content of carbon 15

Korobov Yu.S. Estimation of forces affecting the spray metal in electric arc metallising 21

INDUSTRIAL

Voropaj N.M. Specifics of arc spot shielded-gas welding processes (Review) 26

Kovalenko V.S. and **Kolpakov V.V.** Use of web-technologies to improve the competitiveness of Ukrainian engineering plants 32

BRIEF INFORMATION

Zadorozhny Yu.G. and **Zorin M.I.** Evaluation of mechanical strength of a welded piezotransducer 39

© PWI, International Association «Welding», 2004

STRESSES IN SURFACING OF PARTS MADE FROM HIGH-CARBON STEELS OF THE 65G TYPE AND RISK OF COLD CRACKING

V.I. MAKHNENKO, A.A. GAJVORONSKY, V.A. SARZHEVSKY, E.A. VELIKOIVANENKO, G.F. ROZYNKA and **N.I. PIVTORAK**
E.O. Paton Electric Welding Institute, NASU, Kiev, Ukraine

Conditions of formation of stresses in arc surfacing of high-carbon steel plates are considered from the standpoint of different-orientation cold cracking. It is shown that formation of longitudinal cracks is caused in a number of cases by the presence of peaks of temporary stresses induced by martensitic transformation of austenite.

Keywords: *hardenable steels, welded joints, arc surfacing, martensitic transformation, residual stresses, cold cracks, preheating*

High-carbon steels (C ≥ 0.5–1.0 %) are normally not used in welded structures because of their high susceptibility to hardening and cold cracking [1, 2]. However, welding is widely employed for repair (welding repair of defects, surfacing of worn-out parts, etc.) of different parts of these steels, and in some cases for assembly purposes. In these cases the mandatory standard requirements include performance of preheating to 200 °C and postweld heat treatment, using low-carbon or high-nickel filler metals, and ensuring of a sufficiently low hydrogen content in HAZ [3]. Within the framework of the said general recommendations, in each specific case it is necessary to address the problems associated with selection of technological parameters to provide the required level of quality of a weldment.

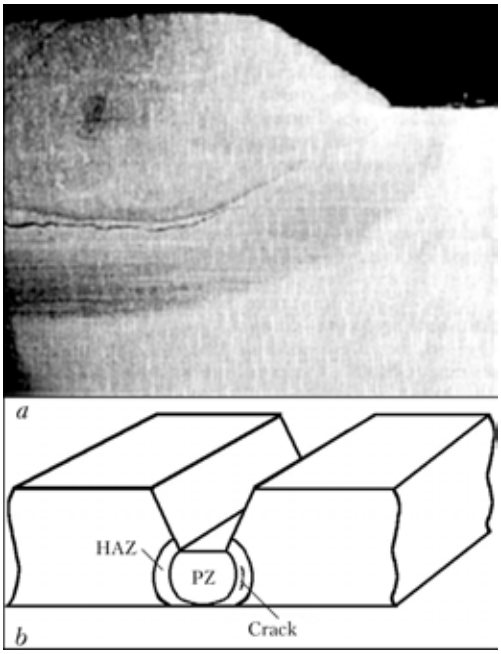

Figure 1. Longitudinal cold underbead cracks formed in surfacing (*a*) and making of a root weld (*b*): PZ — penetration zone

Meanwhile, the range of critical parts from high-carbon steels subjected to welding either for repair or assembly is widening every year. In particular, critical parts of railway transport (rail joints, locomotive and tram wheel tyres, all-rolled wagon wheels, etc.) made from high-carbon steels of the R50, R65, R65K and R75 grades (GOST 51685–2000) are systematically subjected to heating during welding and surfacing. This is done by involving appropriate technological arrangements intended to prevent cold cracking and provide favourable structures of the weld and HAZ metal, as well as mechanical properties of the joints [4–7, etc.].

Despite a great success achieved in investigation of weldability of steels of the above grades, there are still some issues in this field that remain insufficiently studied. Thus, much is unclear concerning conditions of formation of cold cracks depending upon design peculiarities and technological parameters of a welding operation. Formation of cold cracks is known to be caused by four factors [3]: hardening microstructures (martensite or lower bainite), hydrogen, temperature below 150 °C and tensile stresses (as cold cracks are never formed at the absence of high, tensile normal stresses). It is stated in study [3] that the sources of stresses sufficient for the correspondingly oriented cold cracks to be formed can be phase transformations, thermal shrinkage, restraint, external load, sequence of the manufacture of parts, etc. As values of stresses generated by these sources vary during welding, in terms of cold cracking it is important that stresses be present in a corresponding zone at temperature below 150 °C, i.e. in a state close to the residual one. However, this does not mean that in measurement (calculation) of residual stresses one can judge from their values whether the conditions (by stresses) necessary for formation of correspondingly oriented cold cracks are present.

Incorrectness of this premise can be illustrated by an example of formation of longitudinal underbead cracks (Figure 1) formed in deposition of bead on the surface of a high-carbon steel plate of considerable

© V.I. MAKHNENKO, A.A. GAJVORONSKY, V.A. SARZHEVSKY, E.A. VELIKOIVANENKO, G.F. ROZYNKA and N.I. PIVTORAK, 2004

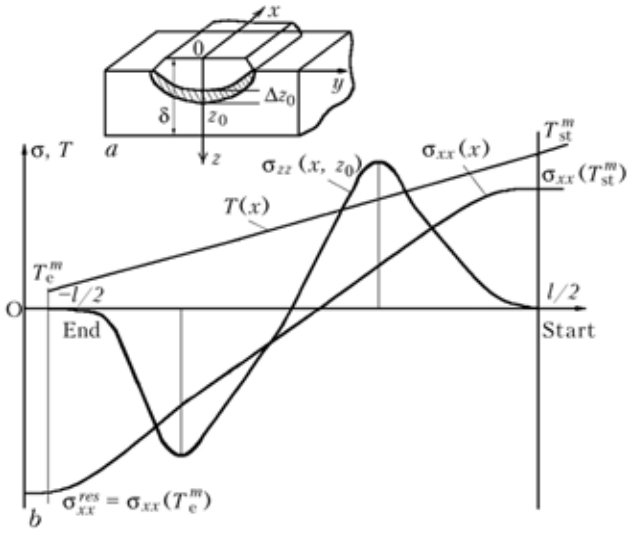

Figure 2. Schematic of the martensitic transformation zone (*dashed region*) (*a*) and curves of distribution of temperature $T(x)$ and stresses $\sigma_{xx}(x)$ and $\sigma_{zz}(x, z_0)$ in the transformation zone $-l/2 < x < l/2$ (*b*)

thickness δ. As shown by measurements and calculations, residual stresses through thickness of the plate are so insignificant in the underbead crack zone that there are no grounds to suggest that they participated in formation of such defects. The most relevant source of stresses is the process of martensitic transformation of austenite occurring non-simultaneously along the bead being deposited. Figure 2, *b* shows schematic that illustrates variations in the martensitic transformation zone $-l/2 < x < l/2$ at $z = z_0$ and $y = 0$ (Figure 2, *a*), temperatures $T(x)$ within a range of $T_{st}^m > T(x) > T_e^m$, and longitudinal, $\sigma_{xx}(x)$, and through thickness, $\sigma_{zz}(x)$, stresses. The peak of stresses σ_{zz}^{max} is proportional to the amplitude of variations of stresses σ_{xx} ($\Delta\sigma = \sigma_{xx}(T_{st}^m) - \sigma_{xx}(T_e^m)$) and inversely proportional to l^2, i.e. it strongly depends upon the properties of a material and process parameters. Given that the HAZ material near the fusion line has usually the lowest crack resistance, which is attributable to an increased content of hydrogen, etc., at sufficiently high values of σ_{zz}^{max} the high probability exists of initiation of an underbead crack and its propagation in direction *x* and along the fusion line, as the $-l/2 < x < l/2$ zone moves along the bead.

Such cold cracks can be conditionally termed the «instantaneous» ones, as the mechanism of «delayed» fracture hardly participates in their formation.

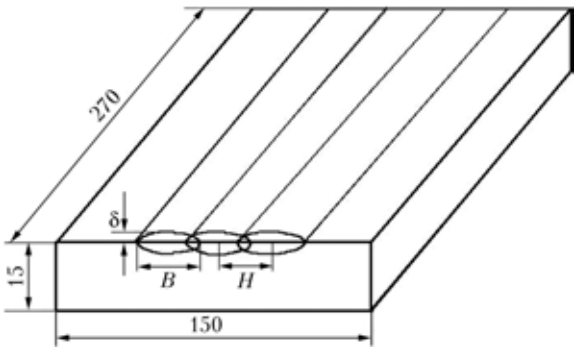

Figure 3. Schematic of deposited specimen: bead width B = 20 mm and deposition pitch H = 18 mm for variant 4; B = 12 mm and H = 10 mm for the rest of the variants

In formation of longitudinal cold cracks of the type shown in Figure 1, *b*, under the effect of transverse stresses σ_{yy}, the source of a corresponding level of transverse stresses, in addition to the known restraint, can also be the above described mechanism of non-simultaneously occurring martensitic transformations, if coordinate *z* is replaced by coordinate *y* in Figure 2, *a*. It is natural that such cracks may propagate both as the instantaneous ones and by the mechanism of delayed fracture. As far as the transverse cold cracks are concerned, their formation is most closely related to the presence of longitudinal residual stresses. However, the factor of formation of a microstructure necessary for such cracks to be formed is often determined by the initial condition of the weld zone (WZ) caused by the initial condition of either metal of the part or previously deposited adjoining bead, rather than by the technological parameters of deposition of a given bead. Transverse cold cracks may also be instantaneous or of delayed fracture.

It follows from the above-said that stresses that cause cold cracking during welding heating of carbon steel parts depend upon a number of circumstances, material parameters and technology employed. So far only a limited amount of the data is available, on the basis of which it is possible to make sufficiently accurate quantitative forecasts. In other words, the area related to weldability of hardenable steels requires in-depth studies, accumulation of concrete results and their subsequent generalisation.

This study presents results of investigation of a particular case, concerning CO_2 arc surfacing of steel 65GS plates 270×150×15 mm in size (Figure 3) performed under conditions indicated in Table 1.

Table 1. Initial characteristics of surfacing variants considered

Variant	*Welding wire*	*Surfacing parameters*			*Preheating* $\dot{O}_0$, $^{i}\tilde{N}$	q_h, *kJ/cm*
		I, A	*U, V*	v_w, *m/h*		
1	Sv-08G2S	160–180	27–28	14.5	20	8.6
2	Sv-08G2S	160–180	27–28	14.5	150	8.6
3	Sv-08G2S	160–180	27–28	14.5	250	8.6
4	Sv-08G2S	160–180	27–28	6.0	20	27.5
5	Sv-08Kh20N9G7T	160–180	27–28	14.5	20	8.6

Table 2. Mean chemical composition (wt.%) of PZ metal

Variant	*C*	*Mn*	*Si*	*Cr*	*Ni*	*P*	*S*	*Mo*	*W*	*V*	*Ti*	*Al*
1.1	0.338	1.345	0.316	0.06	0.06	0.023	0.024	--	--	--	--	0.012
1.3	0.312	1.372	0.316	0.057	0.057	0.022	0.024	--	--	--	--	0.013
2.1	0.370	1.310	0.315	0.064	0.064	0.023	0.025	--	--	--	--	0.014
2.3	0.338	1.345	0.316	0.06	0.06	0.023	0.024	--	--	--	--	0.012
3.1	0.372	1.303	0.315	0.065	0.065	0.024	0.025	--	--	--	--	0.01
3.3	0.346	1.336	0.316	0.061	0.061	0.023	0.024	--	--	--	--	0.012
4.1	0.422	1.255	0.314	0.071	0.071	0.025	0.026	--	--	--	--	0.009
4.3	0.399	1.279	0.315	0.068	0.068	0.024	0.025	--	--	--	--	0.01
5.1	0.338	3.413	0.627	10.64	5.13	0.028	0.018	0.051	0.006	0.04	0.028	--
5.3	0.348	3.335	0.617	10.312	4.973	0.028	0.018	0.049	0.005	0.038	0.027	--

Note. Here and below the second numeral in a variant indicates to the number of deposited bead, e.g. 1.1 — variant 1 and bead 1; 1.3 — same, but bead 3, etc.

Low-carbon wire Sv-08G2S and high-alloy wire Sv-08Kh20N9G7T with a diameter of 1.2 mm were used as the filler metal. Preheating temperature T_0 was varied from 20 to 250 °C. Table 1 gives characteristics of the considered variants of deposition of a single bead and three adjoining beads (Figure 3). In the latter case each next bead was deposited after the temperature that set after deposition of the previous bead decreased to T_0.

Investigations were performed by using the calculation-experimental method. The method provided for estimation of temperature fields and temperature cycles at different points of a specimen, size of PZ and mean chemical composition of its metal, size of HAZ during heating and cooling, and kinetics of mechanical stresses responsible for formation of cold cracks by the mathematical modelling means. The experimental data were used to describe thermal-physical (λ ---- thermal conductivity coefficient, $c\gamma$ ---- volumetric heat capacity) and thermal-mechanical (α ---- thermal expansion coefficient, σ_y ---- yield stress, E ---- elasticity modulus, ν ---- Poisson's ratio) properties, as well as kinetics of microstructural changes in PZ and HAZ, using diagrams of anisothermal decomposition of austenite (variants 1–4) and Schaeffler diagrams (variant 5).

The data on chemical composition of PZ, final microstructure of the PZ and HAZ metal and longitudinal stresses were generated through direct experiments with specimens. The calculation data were compared with those obtained through measurements. Here there is no need to dwell in detail on description of methodological issues of both mathematical modelling and experimental measurements, as the use was made of proven approaches [8–10, etc.].

Consider the results obtained. Table 2 gives the calculation data on a mean chemical composition of the PZ metal for variants 1–5 in accordance with Table 1.

Chemical composition of the PZ and HAZ metal, as well as thermal cycle parameters being known, the authors calculated microstructural transformations for the above zones and kinetics of elasto-plastic strains up to the residual state.

Figures 4 and 5 (see the colour inset) show the results for variant 1.1: cooling time $\Delta t_{8/5}$ at 800–500 °C, relative weight fractions of martensite V_m and bainite V_b, as well as distribution of residual longitudinal stresses σ_{xx}.

Similar results for variants 2.1–5.1 are shown in Figures 6–8 (see the colour inset). As in all these variants the rest of the components of tensor of residual stresses are lower by an order of magnitude (by an absolute value) than longitudinal stresses σ_{xx}, we do not give them here.

Table 3 gives main quantitative characteristics of the calculation results for variants 1.1–5.1 concerning the content of martensite and residual stresses σ_{xx}^{res} in PZ, HAZ and WZ heated below A_{c_3}. It follows from

Table 3. Residual stresses and content of martensite in different zone of welded joints

Variant No.	*PZ*		*HAZ*		*WZ at* $T_{max} < A_{c_3}$	
	V_m	σ_{xx}^{res}, *MPa*	V_m	σ_{xx}^{res}, *MPa*	V_m	σ_{xx}^{res}, *MPa*
1.1	0.90–0.91	65–125	0.85–0.90	–(725–460)	0	865–840
2.1	0.71–0.78	–(71–23)	0.65–0.69	–(730–440)	0	825–755
3.1	0.50–0.52	–(48–20)	0	414–438	0	651–750
4.1	0.20–0.21	660–720	0.16–0.19	276–335	0	725–700
5.1	0	301–363	0.84–0.89	–(650–310)	0	810–853

this Table that in the PZ zone (variants 1.1–4.1), having a substantially lower carbon content than the base metal 65GS (0.66C–1Mn–0.31Si), the martensite content being almost the same, the values of residual stresses σ_{xx} do not decrease far to (see Table 2) the negative range, compared with HAZ, where stresses σ_{xx}^{res} decrease to negative values of –(650–730) MPa.

This phenomenon is caused by occurrence of the martensitic transformation of austenite in the PZ metal in a higher range (here beginning of the martensitic transformation is determined by temperature $T_{st}^{m} \cong$ $\cong$ 360–310 °C, whereas for HAZ of steel 65GS $T_{st}^{m} \cong$ $\cong$ 250 °C). Therefore, compressive stresses σ_{xx} formed during the martensitic transformation in PZ are compensated for during subsequent cooling by temperature shrinkage and subsequent martensitic transformations in HAZ. It is characteristic that in WZ heated below A_{c_3} (see Table 3) stresses σ_{xx}^{res} are higher, and it is here that the highest probability exists of initiation of transverse cold cracks in formation of a corresponding microstructure and mechanical properties of welded joints. In particular, such conditions are very realistic in deposition of adjoining beads with a certain type of overlapping, which is demonstrated in Figure 9 (see the colour inset), which shows distribution of the weight fraction of martensite V_m and residual stresses σ_{xx} after deposition of three adjoining beads (variants 1.3, 2.3 and 5.3). In the selected spot zone the peak values of σ_{xx} are at a level of 1240–1100 MPa (variant 1.3), 1080–950 MPa (variant 2.3) and 1010–970 MPa (variant 5.3). Such spots of a relatively small size may be the centres of formation of small transverse tears or initiation of transverse cold cracks propagating by the mechanism of delayed fracture, when the level of tensile stresses is much lower that the indicated values.

Figure 10 shows the experimental data on delayed fracture of the steel 65GS specimens, which were generated from the tests by the implant method using arc welding parameters as given in Table 1. It can be seen from the Figure that fracture stresses $\sigma_{cr}(t)$ depend upon the welding conditions which determine the microstructural state of HAZ for the given steel.

Table 4 compares values of $\sigma_{cr}(0.1)$ and $\sigma_{cr}(24)$ according to Figure 4, depending upon the martensite content of HAZ (variants 1.1, 2.1, 4.1 and 5.1). It can be seen from the Table that the higher the value of V_m in HAZ of steel 65GS, the lower the resistance to delayed fracture on a base of both 0.1 h and 24 h. The most dramatic decrease in the resistance is seen at $V_m > 0.65$.

Consider the issue of formation of longitudinal cold cracks. Numerical studies by the authors showed that in the $T_{st}^{m} > T(x) > T_{e}^{m}$ temperature range of the martensitic transformation of austenite the peaks of stresses σ_{zz}^{max} (or σ_{yy}^{max}) in HAZ near the boundary with PZ, i.e. at $z = z_0$ and $y = 0$ (see Figure 2), can be

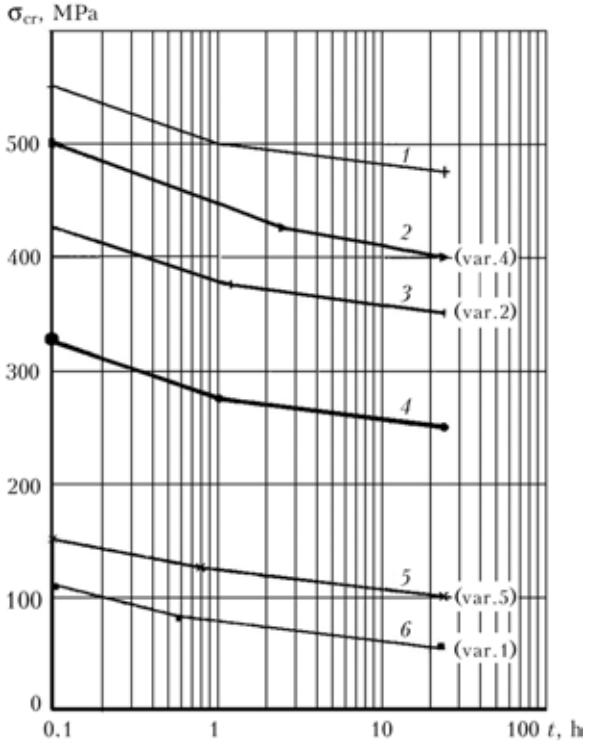

Figure 10. Delayed fracture in HAZ of welded joints in steel of the 65GS type: *1–4, 6* — wire Sv-08G2S; *5* — wire Sv-08Kh20N9G7T; *1, 3–6* ---- q_h = 8.6; *2* — 27.5 kJ / cm; *1* — T_0 = = 200; *2, 5, 6* — 20; *3* — 150; *4* — 100 °C; var.1, 2, 4, 5 — see Table 1

approximately described by the following relationship:

$$\sigma_{zz}^{max} \cong 2.9 \frac{\Delta\sigma}{l^2} z_0^2 f(z_0), \qquad (1)$$

where

$$f(z_0) = 1 + \frac{2\Delta z_0}{z_0} - \frac{z_0}{\delta}\left(1 + \frac{\Delta z_0}{z_0}\right)^2, \qquad (2)$$

providing that the martensitic transformations in PZ $0 < z < z_0$, and HAZ $z_0 < z < \Delta z_0$, occur almost simultaneously, i.e. the difference between temperatures T_{st}^{m} and T_{e}^{m} is not in excess of $0.2(T_{st}^{m} - T_{e}^{m})$.

Otherwise,

$$f(z_0) = 2\frac{\Delta z_0}{z_0}\left(1 - \frac{\Delta z_0}{2(\delta - z_0)}\right). \qquad (3)$$

Table 4. Comparison of critical values of fracture stresses and martensite content of the HAZ metal in some variants indicated in Table 3

Variant	V_m	σ_{cr}, *MPa*	
		0.1 h	*24 h*
1.1	0.89–0.90	110	50
2.1	0.65–0.69	420	350
4.1	0.16–0.19	500	400
5.1	0.84–0.89	150	100

It can be seen from expressions (1) to (3) that the risk of formation of underbead cracks grows with increase in the amplitude of variations of stresses $\Delta\sigma$, ratio z / l, size Δz_0 and thickness δ of a part.

It follows from comparison of (2) and (3) that, other conditions being equal, the use of low-carbon or austenitic steel as a filler in surfacing of high-carbon steel parts leads to a marked decrease in a value of $f(z_0)$ and, hence, σ_{zz}^{max}. It should be noted that the l value in deposition of bead on a massive steel part can be represented in the following form:

$$l \cong \frac{q_s}{2\pi\lambda} \frac{135}{(T_{st}^m - T_0)(T_{st}^m - T_0 - 135)}, \qquad (4)$$

which allows for the fact that $T_{st}^m - T_e^m \cong 135$ °C for many steels [11], and where $q_s = q_h v_w$ is the effective power of a heat source.

As follows from (4), l dramatically grows due to increase in T_0 (at $T_0 \to T_{st}^m - 135$, $l \to \infty$), and, accordingly, the risk of formation of underbead cracks substantially decreases.

CONCLUSIONS

1. Arc surfacing of parts of high-carbon steels of the 65G type induces formation of high tensile longitudinal residual stresses in that part of HAZ where maximal temperatures in deposition of a bead are below A_{c_3}. The presence of such stresses may lead to initiation of transverse cold cracks, if a sufficient amount of martensite is contained in this part of the initial microstructure. This is the case of deposition of adjoining beads with a time interval required for the previous bead to cool down.

2. Underbead cracks are formed during martensitic transformation of austenite in corresponding region z_0 of HAZ or at the boundary between HAZ and PZ under the effect of normal stresses σ_{zz}, which are formed as a result of volumetric effects of the martensitic transformation. Peaks of such maximal stresses σ_{zz}^{max} are proportional to the amplitude of variations of longitudinal stresses σ_{xx} in the $-l/2 > x > l/2$ region of the martensitic transformation and the z_0^2 / l^2 ratio.

3. Preheating to 150 °C excludes any probability of formation of underbead cracks in high-carbon steels.

1. (1974) *Technology of fusion electric welding of metals and alloys*. Ed. by B.E. Paton. Moscow: Mashinostroenie.
2. Makarov, E.L. (1981) *Cold cracks in welding of alloyed steels*. Moscow: Mashinostroenie.
3. (1998) *Welding handbook*. Vol. 4. Materials and applications. Miami: AWS.
4. Sarzhevsky, V.A., Gajvoronsky, A.A., Gordonny, V.G. et al. (1996) Influence of technological factors on structure and properties of HAZ metal in repair-reconditioning surfacing of flanges of all-rolled wagon wheels. *Avtomatich. Svarka*, **23**, 22–27, 33.
5. Kiselyov, S.S., Voronin, N.N., Kuzmina, G.D. et al. (2000) Study of thermal processes and structure formation in twin-arc surfacing of wagon wheels based on computer modelling. *Svarochn. Proizvodstvo*, **3**, 3–8.
6. Kiselyov, S.S., Savrukhin, A.V., Kuzmina, G.D. et al. (1995) Influence of heating during surfacing of all-rolled wagon wheels on residual stresses and strains. *Ibid.*, **12**, 3–7.
7. Dahl, B., Magort, B., Gretoft, B. et al. (1995) Repair of rails on-site by welding. *Svetsaren*, **2**, 10–14.
8. Makhnenko, V.I., Velikoivanenko, E.A., Makhnenko, O.V. et al. (2000) Investigation of the effect of phase transformations on residual stresses in circumferential welding of pipes. *The Paton Welding J.*, **5**, 2–7.
9. Makhnenko, V.I., Velikoivanenko, E.A., Kravtsov, T.G. et al. (2001) Numerical studies of thermomechanical processes in surfacing of shafts of ship mechanisms. *Ibid.*, **1**, 2–10.
10. Taliat, B., Zacharia, T., Wang, X.-L. et al. (1998) Numerical analysis of residual stress distribution in tubes with spiral weld cladding. *Welding J.*, **8**, 328–335.
11. Beres, L. (1998) Proposed to Schaeffler diagram for chrome equivalents and carbon for more accurate prediction of martensite content. *Ibid.*, **7**, 273–276.

MODELING THE CONDITIONS OF PORE INITIATION IN THE WELD METAL IN WET UNDERWATER WELDING

S.Yu. MAKSIMOV[1] and **A.A. GURZHY**[2]
[1]E.O. Paton Electric Welding Institute, NASU, Kiev, Ukraine
[2]Institute of Hydromechanics, NASU, Kiev, Ukraine

Principles of evolution of gas bubbles ahead of the solidification front in wet underwater welding have been investigated using mathematical modeling. Dependence of the effect of solidification rate, hydrostatic pressure and hydrogen concentration on critical radius of a gas bubble and dynamics of its variation have been studied on the basis of the results of the numerical experiment.

Keywords: *underwater welding, pores, modeling, solidification rate, hydrogen, pressure*

Presence of a water medium has a noticeable influence on the process of formation of a welded joint made under the water. The arc runs in a vapour-gas bubble, consisting mainly of water vapours and products of water dissociation. As a result, hydrogen content in the weld metal can reach 55 cm^3 / 100 g, this being much higher than equilibrium content (13.5–14.5 cm^3 / 100 g). In combination with an increased solidification rate and smaller volume of the weld pool, compared to the regular conditions, increased hydrogen content introduces the risk of intensive pore formation in wet welding. On the other hand, higher pressure in the vapour-gas bubble should hinder the process of pore initiation and growth, should increase hydrogen solubility and, therefore, reduce weld porosity [1, 2]. However, by the data of [3, 4], increase of the depth increases the number of pores.

No systematic studies of the features of pore formation in wet underwater welding have been conducted. It is rational to more precisely determine the nature of the influence of factors inherent in wet welding (pressure, solidification rate, hydrogen concentration), on the process of initiation and evolution of the gas bubble in the weld pool. Modern physical methods do not so far permit doing it experimentally, therefore, mathematical modeling is used. Issues of gas interaction with metal have been quite well-studied for the conditions of welding in air [5, 6]. It is established that in the general case the process of pore formation can be divided into two stages, namely nucleation and development of a gas bubble. Its nucleation requires at least three conditions, namely oversaturation of liquid metal with gas, presence of a pore nuclei, and certain soaking of an elementary volume of liquid metal (incubation period) with fulfillment of the above conditions [6]. The most probable area of nuclei formation is the zone adjacent to the interphase [7], as this is where a region of higher concentration of hydrogen dissolved in the metal forms with time. Similar conclusions were drawn by the authors of [8, 9], who used mathematical modeling to study the influence of hydrostatic pressure on the size and shape of the pores in underwater welding. It should be noted that in construction of this model the bubble evolution was considered without allowing for the influence of the solid boundary of «weld pool–base metal» on the diffusion processes in the region adjacent to the bubble [10].

A lot of studies were devoted to evolution of gas cavities [6, 11]. It is found that diffusion phenomena are one of the most important physical processes in the gas–liquid system. Diffusion flow of gas from the liquid into the cavity promotes its collapse, and in some cases the diffusion processes can proceed in such an intensive manner that the gas pressure inside the cavity becomes higher than the external pressure, applied to the bubble surface. As a result, the bubble starts growing. Whether the formed bubble will develop into a pore or not can only be determined, having studied the kinetics of gas distribution ahead of the solidification front and having analyzed the physico-chemical transformations, which proceed on the surface of gas cavities in the molten metal.

This work is devoted to establishing a mathematical model, describing the physical processes proceeding ahead of the solidification front under the conditions of underwater welding. It will permit studying the regularities of evolution of gas bubbles formed ahead of the solidification front under the impact of factors typical for wet underwater welding, determining the main parameters of physical processes causing their further growth, or contrarily collapse of the nuclei in the weld pool. Analysis of the results of the numerical experiment will allow issuing recommendations for selection of the welding modes and technique, promoting prevention or at least retardation of the pore formation process.

Selection of a suitable investigation model largely determines the successful solution of the posed problem. The first significant simplification is the assumption that the solidification front is a flat surface with

© S.Yu. MAKSIMOV and A.A. GURZHY, 2004

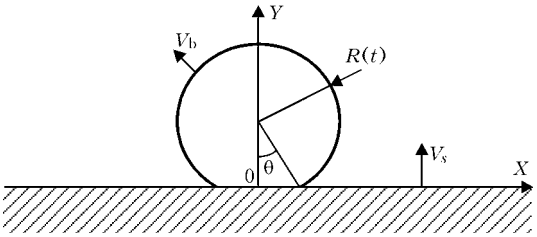

Figure 1. Parameters of a gas bubble (for designations see the text)

a constant propagation rate. Let us assume that gas transport proceeds only through diffusion.

The second group of simplifications pertain to process hydrodynamics. Let us assume that the liquid is quiescent infinitely in the absence of thermal convection, and the liquid proper is ideal and incompressible. We further assume that in the first approximation the impurities dissolved in the liquid do not influence the physical parameters of the liquid medium. We will consider the gas bubble to be uniform and spherical. Use of such simplifications in the considered problem allows applying the known mathematical methods, when solving the hydrodynamic problems, obtaining the results much faster, conducting qualitative and quantitative analyses of the physical processes.

Gas bubble evolution is a transient physical process, occurring under the conditions of considerable local changes of the solidification rates and mass transfer, respectively. The latter should eventually affect the kinetics of the subsurface layer enrichment in gas and the amount of gas diffusing into the cavity.

Let us consider the following problem for study. Let at the initial moment of time $t = 0$ the liquid and solid phases of the metal be separated by a plane — solidification front $y = 0$ (Figure 1). Gas with molecular weight μ and concentration $C(x, y)$ is uniformly distributed in a liquid medium. With time the solidification front and the rectangular system of coordinates (x, y) connected with it move at velocity V_s in the direction of OY axis. At moment of time $t = t_0$ a gas bubble in the form of a truncated sphere with radius R and section angle 2θ forms on the surface of the solidification front. It is necessary to determine the gas bubble parameters with time and conditions for gas cavity formation in the assumption that the gas temperature in it coincides with metal temperature. The latter is valid for equilibrium thermodynamic processes [10].

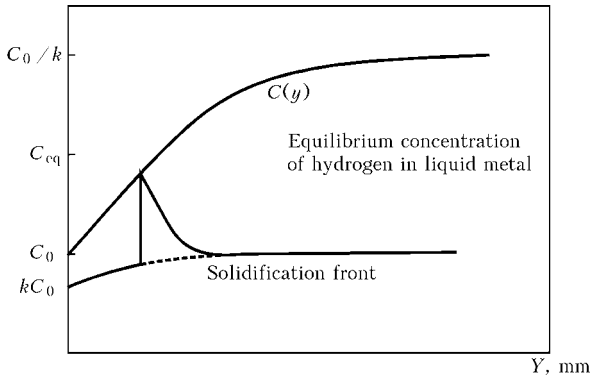

Figure 2. Schematic of hydrogen distribution during solidification (for designations see the text)

Distribution of hydrogen concentration ahead of the solidification front. Assuming on the basis of the results of [8] that hydrogen is the source of porosity in welds made under the water, the condition for bubble formation can be defined as follows: hydrogen concentration in liquid metal C_0 should be above the equilibrium concentration C_{eq}, i.e.

$$C_0 > C_{eq}. \tag{1}$$

Let us assume that near the solidification front there exists a diffusion boundary layer of thickness δ, inside which the mass transfer proceeds only through diffusion, and outside this layer the composition of the liquid metal is kept uniform only due to convection. Hydrogen distribution in the boundary layer in a steady-state solidification mode can be represented in the form of a differential equation [10, 12]

$$D \frac{\partial^2 C}{\partial y^2} + V_s(t) \frac{\partial C}{\partial y} = 0, \tag{2}$$

where y is the distance from the solidification front; D is the coefficient of hydrogen diffusion in liquid metal; $V_s(t)$ is the velocity of displacement of the solidification front.

For the case of V_s = const on the interface in the system of coordinates connected with the moving solidification front, the distribution of hydrogen concentration is defined by the following expression [6]:

$$C(0, t) = C_0 + C_0 \left\{ 1 - \exp\left(-k \frac{V_s^2 t}{D} \right) \right\} \frac{1-k}{k}, \quad t > 0, \tag{3}$$

where k is the coefficient of equilibrium distribution of hydrogen, equal to a ratio of hydrogen concentration in the solid and liquid phases at a given temperature.

Figure 2 schematically shows hydrogen distribution during solidification of the weld pool for a fixed moment t. As is seen from the Figure, even in the case, when hydrogen concentration in liquid metal C_0 is below equilibrium C_{eq}, hydrogen concentration ahead of the solidification front $C(y)$ rises during weld metal solidification and becomes higher than C_{eq} value. At this moment favourable conditions are in place for gas bubble formation.

Hydrogen displacement in the near-boundary layer follows the equation of diffusion

$$\frac{\partial C}{\partial t} = D \Delta C, \tag{4}$$

where Δ is Laplace operator.

After replacement of variables

$$S(y, t) = C(y, t) - C_0 \tag{5}$$

we obtain the following unidimensional problem:

$$\frac{\partial S(y,\ t)}{\partial t} = D\frac{\partial^2 S(y,\ t)}{\partial y^2}. \qquad (6)$$

Solution of equation (6) allows determination of the distribution of the field of hydrogen concentration for arbitrary moment of time t in a point located at distance y from the solidification front:

$$C(y,\ t) = C_0 + C_0\frac{1-k}{k}\left(1 - \mathrm{erf}\left(\frac{y}{2\sqrt{Dt}}\right)\right) - \\ - \frac{2C_0(1-k)\exp\left(-\dfrac{kV_s^2 t}{D}\right)}{k\sqrt{\pi}}\int\limits_{\frac{y}{2\sqrt{Dt}}}^{\infty}\exp(-\eta^2)\exp\left(\frac{kV_s^2 y^2}{4D^2\eta^2}\right)d\eta, \qquad (7)$$

where erf(x) is the error function.

Diffusion processes in the region adjacent to the gas bubble. In the considered problem the «bubble–liquid» boundary is in a continuous regular motion. Its displacement causes the displacement of the adjacent liquid with the gas dissolved in it. In this case the partial time derivative in (4) can be replaced by a total derivative, representing it through the local and convective components. As a result, we obtain the equation of convective diffusion

$$\frac{\partial C}{\partial t} + (\mathbf{U}\cdot\tilde{\mathbf{N}})C = D\Delta C, \qquad (8)$$

where **U** is the velocity field of the liquid flow; ∇ is the differential inverted delta.

Absence of the influence of the impurity on the dynamic aspect of the phenomena is usually assumed — the impurity is regarded to be passive. This assumption can be used only in those dynamic systems, in which the value of concentration of the dissolved substance in the liquid is small [11]. Presence of a non-stationary moving boundary greatly complicates the investigations. However, the influence of the convective component on the diffusion processes cannot be neglected. In this case, the contribution of the convective component into the diffusion equation (8) becomes greater, and under certain conditions it can prevail. Thus, in order to solve the problem, it is necessary to know the flow field, i.e. solve the hydrodynamic problem of a gas bubble motion at a hard flat surface.

Hydrodynamic parameters of the gas bubble in a liquid medium. Let us consider the process of a gas bubble development in an ideal incompressible liquid limited by a half-plane. In the coordinate system, connected with the solidification front, the «liquid–solid phase» boundary is at rest. In this case, the motion of liquid should satisfy equations of Eulerian motion and continuity [10, 11]

$$\frac{\partial \mathbf{U}}{\partial t} + (\mathbf{U}\tilde{\mathbf{N}})\mathbf{U} = -\frac{1}{\rho}\nabla P + \mathbf{F}, \qquad (9)$$

$$\tilde{\mathbf{N}}\mathbf{U} = 0 \quad (\mathrm{div}\ \mathbf{U} = 0), \qquad (10)$$

where ρ is the density; P is the pressure; **F** is the field of external potential forces.

Assuming an absence of vorticity in the boundary layer, we conclude that the following condition is satisfied at any moment of time

$$\tilde{\mathbf{N}}\mathbf{U} = 0 \text{ or } \mathrm{rot}\ \mathbf{U} = 0. \qquad (11)$$

Relationship (11) is a necessary and sufficient condition of potentiality of the velocity field for simply connected domains. As a result, a skalar function $\varphi(x,\ t)$ — the field potential, can be introduced

$$\mathbf{U} = \tilde{\mathbf{N}}\varphi. \qquad (12)$$

After substitution of equation (12) into (11) the potential of velocity satisfies Laplace equation:

$$\Delta\varphi(x,\ y) = 0. \qquad (13)$$

Boundary conditions for equation (13) will be the respective normal components of the velocity field to surfaces limiting the liquid in the system of co-ordinates connected with the solidification front:

$$U_{\mathrm{norm}}(0,\ t) = \frac{\partial\varphi}{\partial y} = 0, \qquad (14)$$

$$\mathbf{U}_{\mathrm{norm}}(x,\ t) = \frac{\partial\varphi}{\partial n} = \dot{r}\ (t), \qquad (15)$$

where $\dot{r}(t)$ is the normal component of the velocity of displacement of a bubble surface.

Proceeding from the fact that the rate of variation of the gas volume in a bubble is proportional to the diffusion flow through an interphase, the equation of material balance of gas in the cavity for a unit of the surface takes the following form:

$$\dot{V} = D\frac{\partial C}{\partial n}\,d\mathbf{S}, \qquad (16)$$

where $d\mathbf{S}$ is the element of bubble surface.

Assuming that the bubble has the shape of a sphere, integration of expression (16) over the entire surface when using the evaluation of gas density [6, 12] becomes

$$\rho = \frac{P_{\mathrm{b}}\mu}{R_{\mathrm{g}}T}, \qquad (17)$$

where P_{b} is the pressure in the bubble; R_{g} is the gas constant; T is the absolute temperature.

The relationship connecting the rate of variation of the gas mass in the bubble with the concentration flow of hydrogen through the bubble surface can be represented as follow:

$$\dot{m} = \frac{P_{\mathrm{b}}\mu D}{R_{\mathrm{g}}T}\oint\limits_S \frac{\partial C}{\partial n}d\mathbf{S}. \qquad (18)$$

Proceeding from the condition of equality of pressures on the bubble surface we can write

$$P_{\mathrm{b}} = P_a + P_{\mathrm{st}}(r,\ \theta) + \frac{2\gamma}{r} = \frac{R_{\mathrm{g}}Tm}{\mu V}, \qquad (19)$$

where $V = C(\theta)r^3 + V_0$, …, $C(\theta) = \frac{\pi}{3}(2 + 3\cos\theta - \cos^3\theta)$ is the cavity volume; P_a is the external pres-

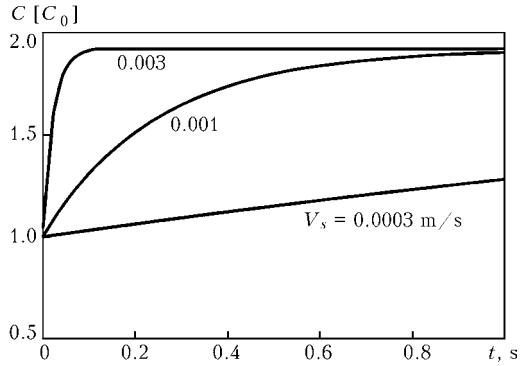

Figure 3. Variation of hydrogen saturation of liquid metal ahead of the solidification front with time at different welding speeds ($D = 1 \cdot 10^{-7}$ m^2 / s)

sure, determined by the depth at which welding is performed; $P_{st}(r, \theta)$ is the static pressure, exerted by the liquid metal on the bubble surface; γ is the coefficient of surface tension; $C(\theta)$ is the coefficient allowing for a reduced volume of the sphere due to the cavity being adjacent to the solidification front; V_0 is the volume of the cavity in the solidified metal; θ is the angle of contact.

Considering the boundary conditions (15) and (16), as well as the flow of hydrogen mass through the cavity surface (18) and balance of forces on its surface (19), for a radial velocity of displacement of the gas bubble surface, we obtain the following expression:

$$\dot{r} = \frac{2R_g T\dot{m} - 2\rho g V_s \mu V}{6R_g T m r^2 / V - \rho g \mu V(1 + \cos\theta_0) - 4\gamma\mu V / r^2}. \quad (20)$$

Thus, the system of equations, describing the model of evolution of a gas bubble located ahead of the solidification front, has closed completely. The obtained system of equations with the respective boundary conditions was the basis of a numerical study of the process of a gas bubble evolution ahead of the solidification front.

Numerical analysis shows that the concentration-induced densification developing during displacement of the solidification front can reach the values of $1.85C_0$, and the thickness of the layer can grow with time up to dimensions of the order of 100 μm (approximately over time 0.5 s). In most of the cases

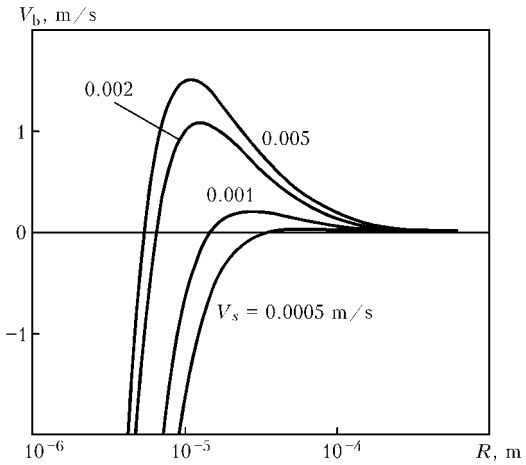

Figure 4. Influence of the solidification rate on the rate of bubble growth ($P_a = 2 \cdot 10^5$ Pa; $\theta = 30°$)

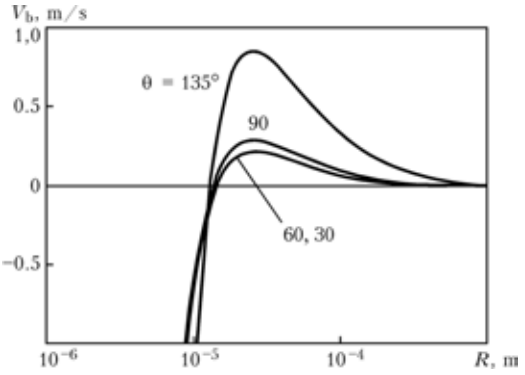

Figure 5. Influence of the contact angle on the bubble growth rate ($P_a = 2 \cdot 10^5$ Pa; $V_s = 0.001$ m / s)

within short time intervals since the moment of a weld pool formation, the gas bubble will collapse because of a low hydrogen saturation of the near-surface layer. Furtheron, when the concentration-induced densification reaches the dimensions of about the size of the gas bubble, the diffusion processes on its surface will lead to a greater saturation of the cavity with gas, and, as a result, to its larger dimensions. Increase of welding speed accelerates the process of the near-surface layer saturation (Figure 3).

Figure 4 shows the dependence of the rate of variation of gas bubble radius V_b on the rate of displacement of the solidification front V_s. Rate of bubble growth rises with increase of solidification rate. This dependence is particularly characteristic of bubbles of a small radius (of the order of 10 μm). At the same time the critical radius R_{cr}, below which the cavity growth rate is negative, also decreases, i.e. the bubble collapses. Rate of growth of large-sized bubbles ($R >$ > 0.5 mm) practically does not depend on the solidification rate, either. In addition, there is a certain solidification rate (in this case, 0.0002 m / s), above which the formed bubble will certainly exist.

Change of the contact angle (angle of contact with the plane solidification front) influences the area of gas bubble surface, the magnitude of which is determined by the rate of the diffusion flows. At increase of the contact angle, starting from $\theta = 60°$, change of the bubble shape becomes noticeable, and its growth rate starts increasing (Figure 5). At $\theta = 135°$ the greater part of the bubble surface is in the hydrogen-enriched layer and, consequently, the rate of its growth rises in the entire range of dimensions.

The developed mathematical model allows tracing all the parameters of the gas bubble with time. Two

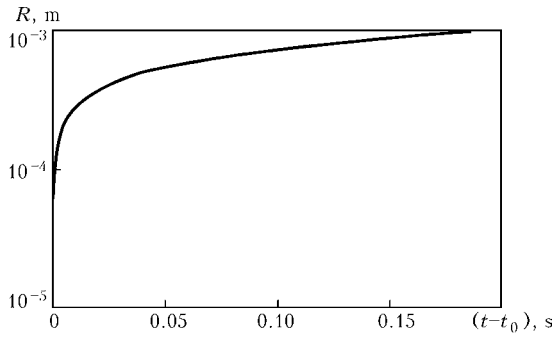

Figure 6. Variation of the gas bubble dimensions during its growth ($P_a = 2 \cdot 10^5$ Pa; $V_s = 0.001$ m / s; $t_0 = 0.2$ s)

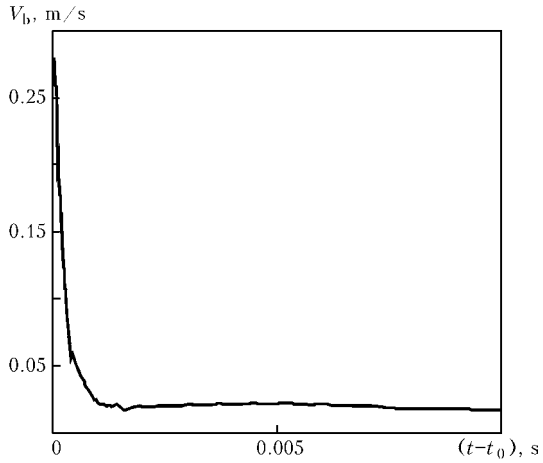

Figure 7. Variation of the rate of gas bubble growth with time (same condition as in Figure 6)

cases were selected as illustrations of the growth (case 1) and collapse (case 2) of the bubble:

Case 1	
R, m	$1 \cdot 10^{-5}$
P_a, Pa	$2 \cdot 10^5$
V_s, m / s	0.001
t_0, s	0.2
Case 2	
R, m	$1 \cdot 10^{-5}$
P_a, Pa	$1 \cdot 10^5$
V_s, m / s	0.001
t_0, s	0.1

In case 1 the region adjacent to the gas bubble, is saturated with hydrogen. Diffusion flow of gas through the surface leads to growth of the gas bubble dimensions (Figure 6). It is interesting to note that increase of the radius by an order of magnitude occurred within 0.2 s. With increase of the dimensions of the cavity, the influence of surface tension is gradually becoming weaker, and pressure in the cavity asymptotically tends to the external static pressure. At expansion, the gas in the bubble cools down. However, its flow through the surface, contacting that of the liquid metal at constant temperature T_0 gradually heats the bubble. With time stabilization of the gas temperature at the level of about 1400 °C is observed. Rate of gas bubble growth depends on hydrogen saturation of weld pool layers adjacent to the cavity. At bubble growth these layers undergo compression, and, therefore, hydrogen concentration decreases. However, for large bubbles the rate of cavity growth decreases (Figure 7). Maximum rate is observed at the initial stage of the growth. On the whole this leads to the conclusion that evolution of gas bubbles is a transient physical process.

In case 2, hydrogen concentration near the solidification front is much lower than in the previous case. This leads to gas diffusion from the cavity into the liquid and reduction of the nuclei radius. At the same time, tension of the adjacent layers of molten metal leads to lower hydrogen concentration in them. Diffusion flow increases even more, and the gas bubble collapses during a short time interval (Figure 8). The collapse process is extremely short, and in our case it takes 0.00001 s, the collapse rate reaching 15 m / s at the final stage. At other parameters it can reach even greater values of 100–500 m / s.

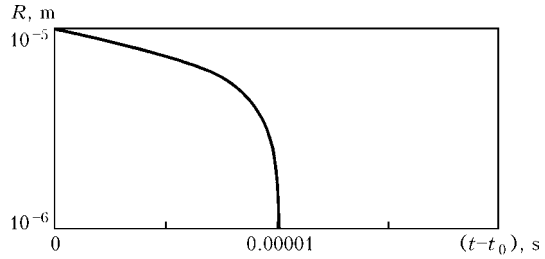

Figure 8. Variation of the dimensions of the gas bubble during its collapse ($P_a = 2 \cdot 10^5$ Pa; $V_s = 0.001$ m / s; $t_0 = 0.1$ s)

CONCLUSIONS

1. Critical parameters of the gas bubble, at which its growth rate is zero, are determined chiefly by external static pressure P_a, rate of solidification front V_s and moment of cavity formation t_0. Critical condition is highly unstable: a slight disturbance of the bubble parameters leads to inevitable growth and collapse of the cavity.

2. Dynamics of bubble growth is determined by the moment of its initiation. The later the bubble forms, the sooner the concentration field in the subsurface layer reaches a high value, this eventually increasing the amount of gas diffusing into the bubble cavity and promoting the growth of the bubble.

3. Dynamic characteristics of the gas bubble ahead of the solidification front are largely dependent on the velocity of motion of the flat front practically in the entire range of the possible initial radii of the gas bubble. With increase of the rate of the solidification front, the diffusion processes proceed faster, and the critical parameters of gas bubbles shift into the region of smaller dimensions.

1. Ando, S., Asahina, T. (1983) A study on the metallurgical properties of steel welds with underwater gravity welding. In: *Proc. of Int. Conf. on Underwater Welding*, Trondheim, June 27–28, 1983. Oxford.
2. Ibarra, S., Olson, D.L., Liu, S. (1991) Effect of water depth on underwater weld metal porosity formation. In: *Proc. of Int. Conf. on Underwater Welding*, New Orleans, March 20–21, 1991. Miami: AWS.
3. Szelagowski, P. Underwater wet welding. In: *SCUW 127–90*.
4. Olson, D.L., Ibarra, S. (1986) Underwater welding metallurgy. In: *Proc. of 1st Conf. on OMAE*. 1986.
5. Pokhodnya, I.K., Taraborkin, L.A. (1986) Mathematical modeling of behavior of gases in the weld pool. In: *Metallurgical and technological problems of flux-cored wire welding*. Proc. of Int. School of CIS countries on Flux-Cored Wire Welding, Sofia, April, 1986. Kiev: Naukova Dumka.
6. Pokhodnya, I.K., Demchenko, V.F., Demchenko, L.I. (1979) *Mathematical modeling of behavior of gases in welds*. Kiev: Naukova Dumka.
7. Pokhodnya, I.K. (2002) Control of hydrogen in weld metal. In: *Problems of corrosion and corrosion protection of materials*. Spec. Issue 3, Vol. 1. Lviv: FKhMM.
8. Suga, Y., Hasui, A. (1986) On formation of porosity in underwater weld metal. Part 1. Effect of water pressure on formation of porosity. *Transact. of JWS*, 17(**1**), 58–64.
9. Suga, Y. (1987) On formation of porosity in underwater weld metal. Part 2. Study on mechanisms of blowhole formation by hydrogen. *Ibid*., 18(**1**), 61–68.
10. Landau, L.D., Lifshits, E.M. (1986) *Hydrodynamics*. Moscow: Nauka.
11. Lojtsyansky, L.G. (1986) *Mechanics of liquid and gas*. Moscow: Nauka.
12. Flemings, M. (1977) *Solidification processes*. Moscow: Mir.

EFFECT OF HEAT TREATMENT AND DEGREE OF ALLOYING ON STRUCTURAL CHANGES IN NICKEL ALLOYS

K.A. YUSHCHENKO, V.S. SAVCHENKO and **A.V. ZVYAGINTSEVA**
E.O. Paton Electric Welding Institute, NASU, Kiev, Ukraine

Alloys with a different content of γ′-forming elements have been studied. High-temperature ductility of heat-resistant nickel alloys with a different content of γ′-forming elements after heat treatment at a different cooling rate has been evaluated. It has been established that heat treatment allowing to control growth of the γ′-phase is indicated only for alloys with a high degree of alloying.

Keywords: *nickel alloys, γ′-forming elements, heat treatment, cooling rate, high-temperature ductility, microstructure, dilatometer, phase transformations*

Modern heat-resistant alloys have complex structure and alloying system. They have an increasingly wide application, which is associated, first of all, with the possibility to achieve a substantial strengthening effect and maintain structural stability at high temperatures.

Microstructure of cast heat-resistant nickel alloys is a matrix with the fcc lattice, containing carbides and a coherent intermetallic γ′-phase, which is the main strengthening phase. Structural stability and behaviour of the γ′-phase at high temperatures and a long holding time determine to a considerable degree performance of an alloy. Firstly, particles of the γ′-phase may dissolve in structure of heat-resistant alloys at increased temperatures, and volume content of this phase may decrease to a value corresponding to the equilibrium one at a given temperature; secondly, the remaining particles may change in size as a result of coagulation. Kinetics of these two processes is controlled by a diffusion transfer of atoms in γ-solid solution [1, 2].

There are alloys with a low content of γ′-forming elements (aluminium, titanium, etc.), for which the temperature of full dissolution of the γ′-phase, $T_{f.d}$, can be lower than the temperature of formation of coarse particles of the γ′-phase. Working level of service temperatures of units and components of these alloys is rather low (~ 750 °C).

Increase in the content of alloying elements and, hence, amount of the γ′-phase from 10 to 55 % leads to a substantial increase (of about 250 °C) in temperature level of operation of nickel alloy parts [3, 4].

For alloys with an increased content of alloying elements, the process of dissolution of the γ′-phase shifts to a range of high temperatures. The higher the temperature of dissociation of the oversaturated solid solution and the higher the level of $T_{f.d}$, the higher the intensity of occurrence of the diffusion processes and the coarser the redundant phase [5]. The amount of coarse precipitates of the γ′-phase also depends upon the cooling rate and temperature of the end of slow cooling from the range of high temperatures.

Increased content of alloying elements, such as aluminium, titanium and niobium, which have a limited solubility in the nickel matrix, causes high chemical heterogeneity of metal and widening of temperature range of a solid-liquid state in solidification. Increase in operational ductility of metal leads to improvement of weldability. Properties of metal can be changed through controlling its structure and, first of all, size of the γ′-phase [6]. Overageing of metal is a technological operation that increases ductility and decreases strength by a controlled growth of redundant phases. This can be achieved by applying special heat treatment, providing coarse precipitates of the γ′-phase, the size of which depends upon the cooling rate and temperature of the end of the slow cooling process.

As seen from the above-said, it is of interest to study the effect of heating and cooling on structure and ductile properties of alloys with a different content of alloying elements and, hence, different content of the γ′-phase.

Five alloys with a different content of γ′-forming elements were studied. The degree of alloying with the γ′-forming elements and content of the γ′-phase in alloys studied are given in the Table.

For alloy 3, the amount of the γ′-phase was determined by the method of X-ray diffraction analysis

Content of γ′-forming elements in experimental heat-resistant alloys with a different content of the γ′-phase

Alloy	*Al + Ti + Nb + Hf, %*	*Content of γ′-phase, %*
1	2.44	8.2
2	6.60	38.6
3	7.70	47.3
4	8.19	49
5	9.50	57

© K.A. YUSHCHENKO, V.S. SAVCHENKO and A.V. ZVYAGINTSEVA, 2004

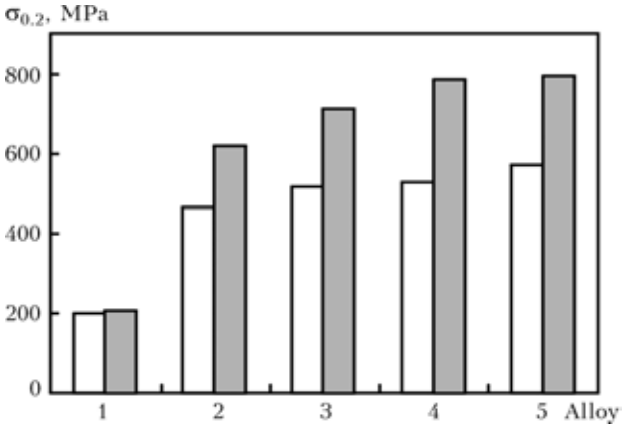

Figure 1. Yield stress of alloys with a different degree of alloying depending upon the heat treatment: *white columns* — experimental; *grey columns* — standard

using the «Dron-3» machine, and it was 44.6 %, which is in agreement with literature data [3].

To determine the amount of the γ'-phase in alloys given in the Table, differential thermal analysis (DTA) was performed using a high-temperature vacuum dilatometer with a non-contact system for measurement of the longitudinal displacement of a specimen. Specimens were heated to a temperature of full dissolution of the γ'-phase, and then the exothermic process of precipitation of the γ'-phase was fixed on a cooling branch. The amount of the γ'-phase can be calculated from the proportions of areas under the peaks of the curves, providing that specimens of all the alloys have an identical mass.

Heat treatment was conducted in air-tight containers filled with argon, which were placed into an electric furnace using SiC rods as a heater. Working temperature amounted to 1350 °C. Specimens were heated to a temperature a bit higher than the temperature of full dissolution of the γ'-phase to study the effect of the cooling rate on ductile properties of nickel alloys. Then one batch was cooled at a slow rate, while the other was subjected to forced cooling in air.

Device for ion etching in a high-voltage glow discharge, using the VUP-4 machine, was employed to reveal structure of the specimens. In contrast to chemical etching, this type of treatment allows etching out of the grain boundaries to be avoided, as well as carbide and intermetallic inclusions to be revealed more clearly. Argon was used as a working gas for the glow discharge. Subsequent high-temperature etching in dynamic vacuum provides a more accurate identification of structural components of an alloy.

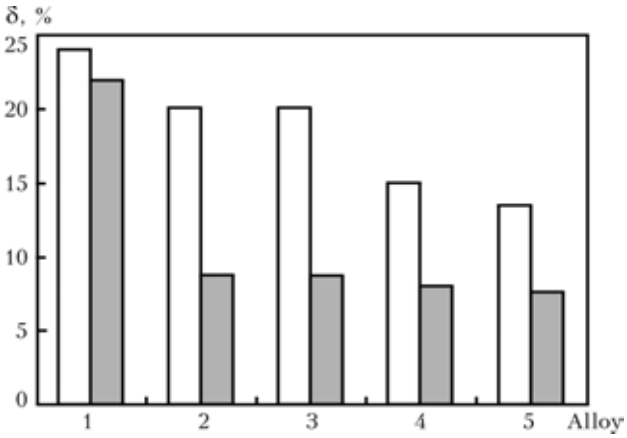

Figure 2. Ductility of alloys with a different degree of alloying depending upon the heat treatment: *white columns* — experimental; *grey columns* — standard

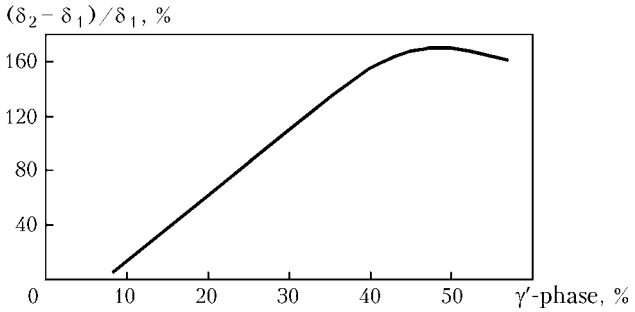

Figure 3. Relative variation in ductility at experimental heat treatment of nickel alloys with a different content of the γ'-phase

High-temperature ductility δ and yield stress $\sigma_{0.2}$ were estimated using the ALA-TOO testing machine in a vacuum chamber at residual pressure of $1 \cdot 10^{-3}$ MPa and temperature of 750 °C. Specimens with a cross section of 4 mm^2 were used for the tests.

Analysis of the results (Figure 1) shows that the yield stress value increases and difference between the values of $\sigma_{0.2}$ of the quenched and overaged specimens grows as the alloying system becomes more complex.

For the quenched specimens, ductility falls to a larger degree than for the overaged ones (Figure 2).

The similar trend is fixed in Figure 3, which shows relative variation in ductility resulting from the experimental heat treatment, depending upon the amount of the γ'-phase, which was determined from the DTA data. The dilatometry examinations showed increase in $T_{f.d}$ with increase in the degree of alloying. Specimens of the alloys studied were heated to a temperature of full dissolution of the γ'-phase. Structural changes accompanied by decrease in the metal volume were detected to occur in cooling of these specimens.

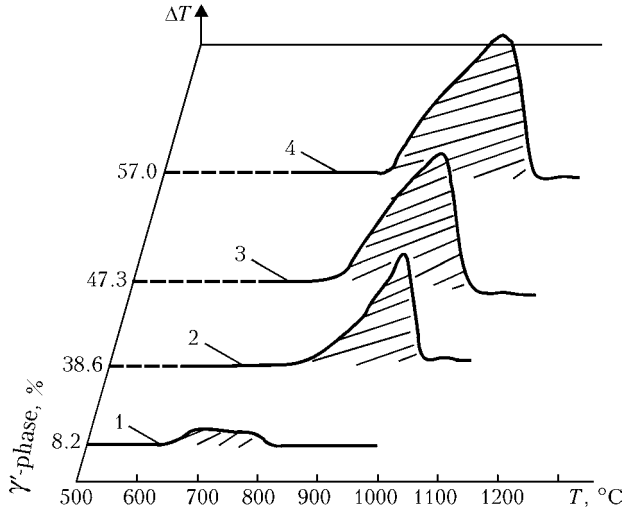

Figure 4. Curves for exothermic reactions of formation of the γ'-phase in alloys 1–4: area under a curve is proportional to the amount of the precipitating phase; T — heating temperature

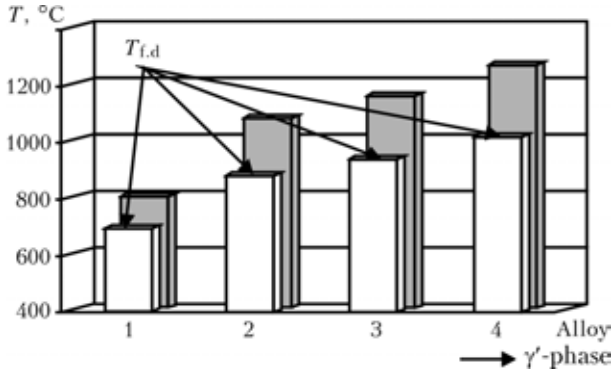

Figure 5. Histogram of dissolution of the γ′-phase depending upon the degree of alloying of an alloy: *white columns* — beginning; *grey columns* — end of transformation

This is indicative of precipitation of the γ′-phase, which has a smaller crystalline lattice parameter, compared with the γ-solid solution. As follows from the results of the studies (Figure 4), increase in the amount of γ′-forming elements favours increase in temperature *T* of the transformation beginning and end, as well as increase in volume of the precipitated phase.

The DTA data make it possible to plot a histogram (γ–γ′) for alloys with a different content of alloying elements. It can be seen from this histogram that increase in the degree of alloying of an alloy due to increase in the content of aluminium and titanium leads to growth of the temperature of full dissolution of the γ′-phase, as well as growth of an interval between the temperature of the beginning and end of the process of dissolution of the γ′-phase due to increase in the amount of the phase that undergoes transformation (Figure 5).

Microstructure of the precipitation-hardening alloy IN 738LC was examined in view of the detected difference in data depending upon the type of heat treatment for specimens with an increased content of alloying elements and a large amount of the γ′-phase. After all types of heat treatment, the structure (Figure 6) comprised the γ-matrix solution with a large amount of the γ′-phase from 0.07 to 0.85 μm in size, depending upon the heat treatment. Coarsening of the γ′-phase was accompanied by decrease in hardness. As shown by the measurements, hardness of the alloy in the as-received condition was *HRC* 36.3, while after the experimental heat treatment it decreased to *HRC* 32.

Phase transformation (for non-overaged specimens) results in formation of chaotically distributed precipitates of the γ′-phase, the mean size of which is approximately 0.07 μm. After overageing, only the coarse particles (70–85 μm) are formed in the alloy. The volume content of precipitates of the γ′-phase was estimated using the point-by-point analysis method. It was 44–47 % for alloy 3, which is in good agreement with the data of X-ray diffraction analysis performed using the «Dron-3» machine. Statistical data on sizes

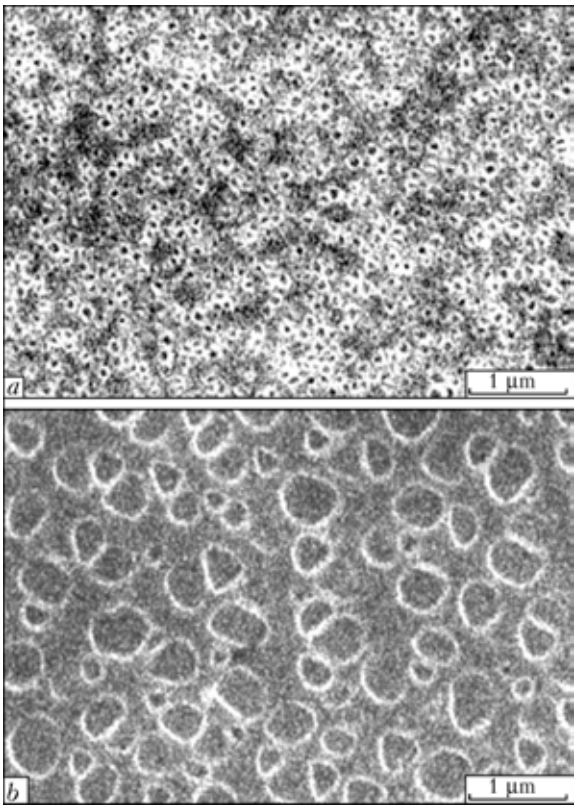

Figure 6. Microstructure of the surface of alloy 3 depending upon the heat treatment: *a* — rapid cooling; *b* — slow cooling

and quantity of particles were generated from different regions of a specimen (about 100 measurements).

Dispersed particles (0.07–0.1 μm) of the γ′-phase block dislocations (low ductility). Coarsening of the γ′-phase particles facilitates realisation of plastic deformation by the mechanism of bending of the dislocations around the γ′-phase particles, which raises the ability of the alloy to be plastically deformed [7].

CONCLUSIONS

1. It was established that in heat treatment of welded joints it is necessary to allow for the dependence of temperature of full dissolution of the γ′-phase upon its content.

2. It was found that the operational ductility of nickel alloys can be controlled through varying the γ′-phase content.

1. (1995) *Superalloys II*. Ed. by R.E. Shilin. Moscow: Metallurgiya.
2. Hiroshi, H. (1979) Series superalloy on IN 713C base on the cut γ–γ′. *J. Iron and Steel Inst. Jap.*, 65(**7**), 1049–1058.
3. Watanabe, R., Tsuneo, K. (1975) Alloy design of nickel-base precipitation hardened superalloys. *Ibid.*, 61(**9**), 126–146.
4. Stroganov, G.B., Chepkin, V.M. (2000) *Cast heat-resistant alloys for gas turbines*. Moscow: ONTI-MATI.
5. Lashko, N.F., Zaslavskaya, L.V., Kozlova, M.N. et al. (1970) *Physical-chemical methods for phase analysis of steels and alloys*. Moscow: Metallurgiya.
6. Gessinger, G.H. (1988) *Powder metallurgy of heat-resistant alloys*. Chelyabinsk: Metallurgiya.
7. Sims, C.T., Hagel, W.C. (1972) *Superalloys I*. New York: J. Wiley & Sons.

MORPHOLOGICAL PECULIARITIES OF MICROSTRUCTURE OF WELD METAL FROM LOW-ALLOY STEELS WITH ULTRALOW CONTENT OF CARBON

V.F. GRABIN, V.V. GOLOVKO, V.A. KOSTIN and **I.I. ALEKSEENKO**
E.O. Paton Electric Welding Institute, NASU, Kiev, Ukraine

It is shown that in addition to the ordinary structures characteristic of welds hardened due to presence of pearlitic structures, welds with an ultralow carbon content also develop various ferrite morphologies, including an unusual form of laminar Widmanstatten ferrite, as well as massive forms of ferrite which solidify in the form of dendrite or as a «conglomerate» of round-shaped crystallites, separated from each other by boundary precipitations of MAC-phase, forming at the final stages of residual austenite decomposition. It is noted that to decrease the carbon liquation into weld metal its silicon content should not be higher than 0.3 wt.%.

Keywords: *low-alloy steels, weld metal, evolution of ferrite, polygonal ferrite, acicular ferrite, Widmanstatten ferrite, massive ferrite, MAC-phase, structural constituents*

At the second half of the XX century the production of low-alloy steels was developing very rapidly. Since 1985 to 2000 their production in the world was increased from 50 to 830 mln t per year. This level of consumption was stipulated by optimum ratio of economical efficiency and service properties. Especial significant achievements in the field of production of high-strength sparsely-alloyed steels were attained over the recent quarter of the century when it was possible, owing to fundamental studies, to make progress in the solution of such problem, which seemed as contradictory for the development of steels with simultaneously increased characteristics of strength and ductility.

The main hardening element of low-alloy steels is carbon, however, it is the element that promotes the formation of quenched structures and different carbide phases in metal, that can cause the reduction in its ductile properties and resistance against brittle fracture. To avoid this negative effect of carbon it is rational to decrease its content in metal by using firstly the converter, and then electric arc method of steel production. Here, it was possible to reduce the carbon content in metal to the ultralow level (less than 0.05 wt.%). In this case the preset level of strength is attained by alloying metal with chromium, nickel or manganese. In steels with an ultralow content of carbon (ULCC) the level of strength ($\sigma_t \cong$ $\cong$ 820 MPa), ductility ($\delta \geq 20$ %) and impact strength ($KCV_{-60} \geq 60$ J / mm^2) are well correlated, due to which they are characterized by a low susceptibility to brittle fracture [1].

Steels with ULCC are characterized, as compared with low-alloy high-strength steels, by higher resistance against brittle fracture. It is known [2, 3] that in steel with ULCC the traditional forms of microstructures, based on ferrite and cementite, are replaced mainly by a ferrite structure, but here its morphological forms are somewhat differed from those formed usually in steel with higher content of carbon. Proceeding structural changes are accompanied by the formation of ferrite forms, known and unusual for the researchers. This is a number of conventional morphologies of ferrite which are formed at low rates of cooling with the formation of polygonal (hypoeutectoid) and Widmanstatten ferrite, defined comparatively easily by a light microscope, and also martensite-like phases. It is possible to obtain other modifications of ferrite within the range of intermediate rates. These are such forms of ferrite which are not observed usually in welds, for example, laminar forms of ferrite precipitations with a different orientation; they were called earlier bainitic or «probainitic» ferrite. At present different forms of this ferrite by classification of IIW are called a ferrite with ordered and disordered second phase. It should be noted that until now there is no clear differentiation of ferrite structures, formed in the intermediate area, the boundary of formation of martensitic-austenitic-carbide (MAC) phase and its forms are not defined, many other problems connected with the kinetics of transformation in the intermediate area are not elucidated. In spite of great attention paid and continued to be paid to this problem, the classification of structure constituents has not been yet finalized.

Physical-mechanical properties of low-alloy steels of high-strength welds with ULCC depend greatly on content of carbon in them, as the sensitivity of different types of microstructures to the kinetic factors, defining their growth, becomes much higher in reduction of its mass share [2]. An additional factor influencing the physical-mechanical properties of weld metal, is the steel alloying with manganese, molybdenum, nickel and some other elements to provide an acceptable level of strength. Complex of fer-

© V.F. GRABIN, V.V. GOLOVKO, V.A. KOSTIN and I.I. ALEKSEENKO, 2004

Table 1. Chemical composition of weld metal, wt.%

Number of weld	C	Si	Mn	Mo	Ni	Al	Ti	Cr	Cu	P	S
1	0.025	0.10	0.62	0.15	2.29	0.014	0.003	0.17	0.12	0.013	0.006
2	0.037	0.09	0.99	0.51	2.25	0.018	0.003	0.19	0.12	0.014	0.005
3	0.048	0.46	0.99	0.30	1.87	0.012	0.008	0.24	0.30	0.009	0.014
4	0.073	0.42	1.28	0.27	1.27	0.013	0.013	0.28	0.40	0.016	0.010

rite-cementite structures, forming in this case, does not always provide the required resistance of welds against the cold crack formation.

Development of welding consumables and technologies for manufacture of structures from steels with ULCC is impossible without study of specifics of formation of microstructure of the welded joint metal. The present work deals with the results of study of new and modified forms of ferrite, peculiarities of their morphology and composition, and also the role of MAC-phase forming in the deposited metal in welding with alloyed welding wire having ULCC.

During the works conductance the attention was paid to the MAC-phase, as some researchers [4–6] associate its presence with the susceptibility of welded joints to the brittle fracture. Using electron microscopy and magnetic methods of examination it was established that MAC-phase is a complex phase consisting of a mixture of structureless martensite, bainite and residual austenite [7–9]. Authors of the mentioned works stated that the areas of bainite particles represent a ferrite-carbide mixture of high dispersity, due to which they are coloured darker and more uniform than those of structureless bainite. Content of MAC-phase in welds made on low-alloy steels can vary in the 1.5–12.0 wt.% range, depending on the heat input, and the maximum content of residual austenite in it does not exceed 4.5 vol.%. Microhardness of this phase in low-carbon steels is 4500–5700 MPa [7]. In some other works [10–12] the higher values of microhardness of MAC-phase, 8000–8500 MPa, are given, that assumes the high content of carbon in it.

Material and procedure of investigations. Butt joints of samples of metal of multilayer welds (deposited metal) made in accordance with requirements of the European standard EN 1597-1 on steel 10XSND using highly-basic neutral flux ANK-57 (DIN 32 522; BFB 155; DC 8; KMHP 5) in combination with welding low-alloy wires, having ULCC, were selected as an object of investigations. The selection of type of welding wire was defined by the task of producing weld metal with different content of carbon, nickel, molybdenum.

Welding was performed at direct current of reverse polarity at the following conditions: $I_w = (620 \pm 5)$ A; $U_a = (30 \pm 1)$ V; $v_w = (20 \pm 0.5)$ m / h; $q_w =$ = 48 kJ / cm. Rate of weld cooling was at the level of 4–7 °C / s. Chemical composition of metal of welds is given in Table 1.

Areas, corresponding to the last pass in the weld upper part, which were subjected to repeated heating, were examined.

Identification of structural constituents in weld metal was realized by using etching in nithal and alkali solution of sodium picrate and measurement of microhardness. Calculation of volume shares of structure constituents was made by a traditional point-by-point method using a grid of 81 cells with magnification 500 (after etching in nithal) and 1000 (after etching in sodium picrate). This procedure of investigation allowed reliable sufficient identification of phase composition of microstructure of weld metal and obtaining data about the quantitative its ratio of separate structural constituents (Table 2).

Results of experiment. Microstructural investigations showed that the weld metal of samples consists of phases representing a ferrite of different morphological forms, such a polygonal ferrite (PF), Widmanstatten ferrite (WF), acicular ferrite (AF), laminar ferrite (LF). Morphology of forming microstructures is stipulated by a size, orientation, shape of ferrite grains, and also by a mutual arrangement of ferrite and carbide phases.

The effect of carbon content in weld metal on the volume share of structural constituents in it is given in Figure 1. With decrease in carbon content in weld metal the volume share of AF, PF and MAC-phase is reduced, while LF is increased. The content of WF of a usual shape remains almost at the same level, i.e. 0–4 vol.%.

A form of ferrite was revealed in the weld metal, called quasi-polygonal in [13] and formed in the form of wide laminas growing normal to the boundaries of austenitic grains (Figure 2). This type of structure can be considered, coming from the direction of growth of its grains, as precipitations of WF, though its appearance differs from a classic form typical of

Table 2. Structural composition of weld metal, vol.%

Number of weld	Polygonal ferrite	Widmanstatten ferrite	Acicular ferrite	Laminar ferrite	MAC-phase
1	5	3	35	49	2.4
2	4	4	40	46	3.3
3	17	3	45	31	4.0
4	15	–	73	35	6.4

Note. Bainite was not revealed in weld metal.

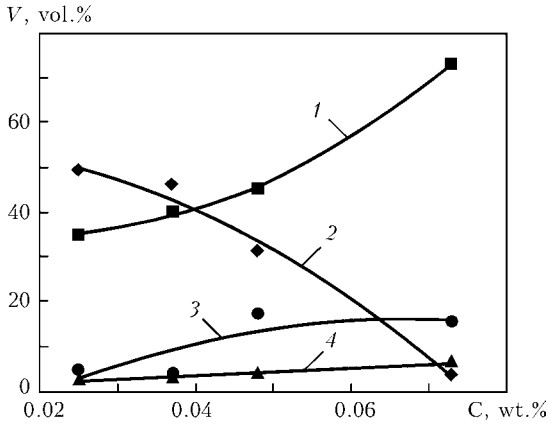

Figure 1. Effect of carbon content in weld metal on volume share of structural constituents, *V*: *1* — AF; *2* — LF; *3* — PF; *4* — MAC-phase

microstructure of the latter with the higher carbon content.

Two massive morphological forms of ferrite, which are differed from the known forms by the nature of precipitations, were revealed in the microstructure of weld metal with ULCC: one of them has a form of dendritic crystals, another one has a form of «conglomerate» of ferritic crystals of an irregular shape (Figure 3).

The growth of a structural phase in a solid state in the form of crystals of a dendritic shape is unusual, but known [14]. It was observed in precipitation of excessive cementite in the process of decomposition of overcooled austenite in cast irons. In the opinion of the author of [14], the formation of dendritic shapes of forming regions of this phase is stipulated by its crystalline nature and difference in rates of growth of different crystallographic facets. Differences in rates of growth of separate regions of surface of the new phase (ferrite) is undoubtedly connected with different intensity and conditions of proceeding diffusion processes in adjacent volumes of austenite. AF (Figure 3, *a*, *b*), being a product of decomposition of microregions of overcooled austenite, enriched with carbon, is located in gaps of interdendritic spacings of these crystallites.

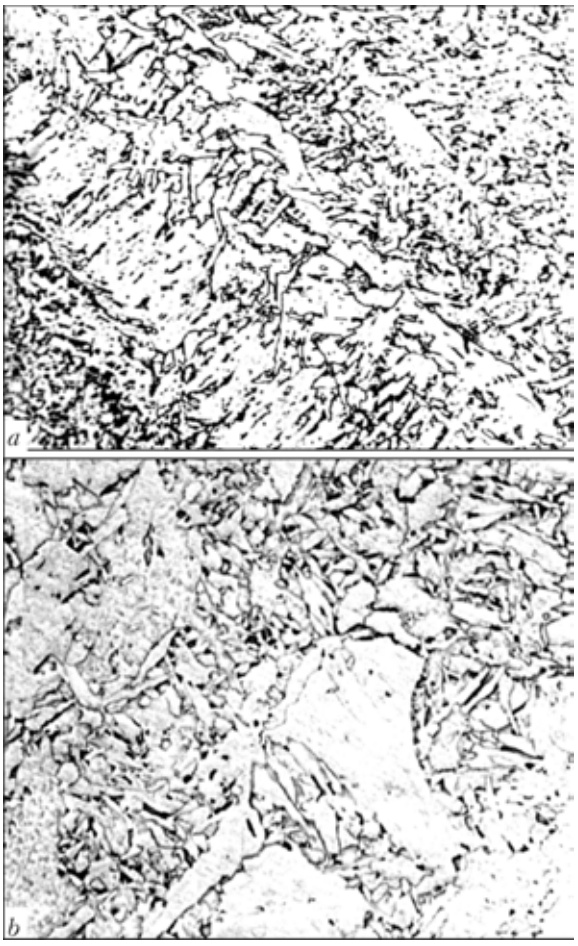

Figure 2. Microstructure of ferrite of quasi-polygonal form obtained using optic (*a* ---- ×320) and scanning (*b* — ×1300) microscopy

Massive precipitations of the ferrite phase in the form of «conglomerate» are observed more seldom and represent a group of ferritic crystals of irregular shape which are precipitated due to the presence of dark dispersed precipitations between them. These precipitations are classified as MAC-phase.

Analysis of results. As is known, PF is the first phase which is formed in the process of weld cooling during decomposition of the overcooled austenite.

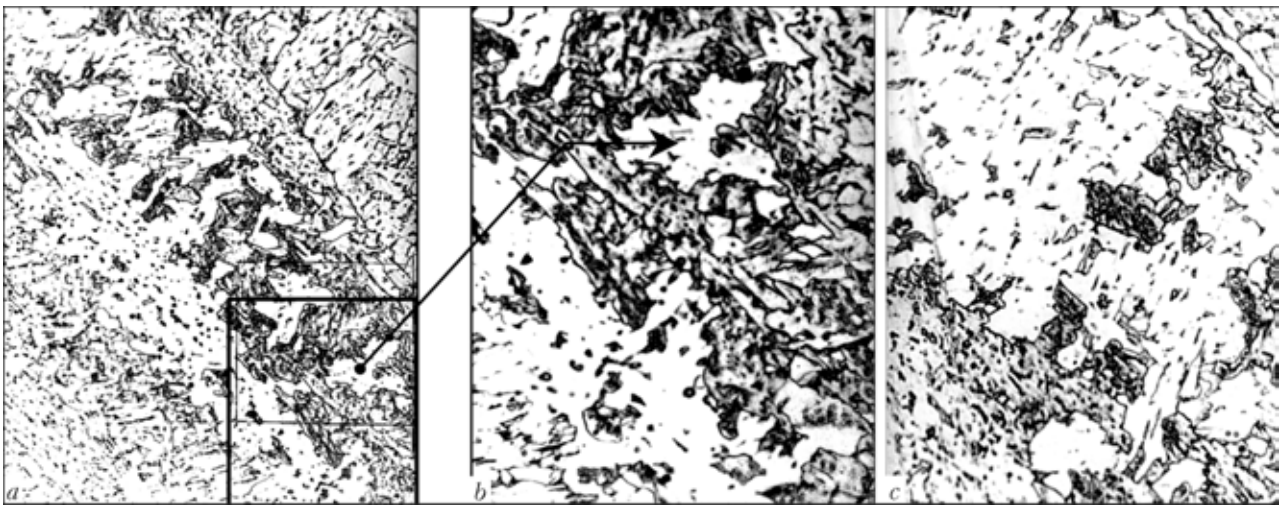

Figure 3. Morphological forms of massive ferrite: *a*, *b* — dendritic forms (×1000 and ×2000, respectively); *c* — «conglomerate» of ferrite crystallites (×2000)

Table 3. Mass share of alloying elements in ferrite, %

Form of ferrite	*Si*	*Ti*	*Ni*	*Mn*	*Mo*
MF	0.420	0.071	1.981	0.686	0.227
PF	0.327	0.057	1.926	0.764	0.162
AF	0.269	0.069	1.879	0.702	0.054

This form of ferrite is originated usually at the boundaries of austenite grains in the form of allotriomorphs, i.e. grains, not having a regular geometric form due to non-equilibrium conditions of growth. The PF precipitations are thickened in the direction normal to the austenite grain boundary [2]. Thickness of PF grains depends on the rate of carbon diffusion and should increase with the carbon content decrease in it. However, we have received the contrary relationship (see Figure 1).

This result and the fact, that the weld metal has ULCC, give grounds to assume the following: in the present case the structure formation is affected greatly not by carbon, but by other alloying elements.

The effect of alloying on PF content is manifested in shifting the critical point of alloy A_{c_3}. It is known that metal alloying with such elements as manganese, nickel, molybdenum and copper, promotes the reduction in critical rate of hardening [15, 16] and increase in degree of the austenite overcooling. This results in decrease of intensity of PF origination. Otherwise, the presence of silicon and aluminium increases A_{c_3} and, respectively, increases the rate of initiation and growth of the ferrite phase.

It should be noted that the conditions of proceeding reactions of formation of PF are affected greatly, except the system of alloying, by such parameters as a size of austenite grain, rate of weld metal cooling within the temperature region of the least stability of austenite and nature of distribution of non-metallic inclusions. All this affects not only the PF formation, but also the sequence of formation of other structural components in the process of $\gamma \rightarrow \alpha$ transformation. With increase in rate of metal cooling the content of microstructural constituents, forming by the diffusion mechanism (PF and MF ---- massive ferrite) is decreased in it and the share of AF and MAC-phase is increased, i.e. those structural constituents which were formed by a diffusion-free mechanism of transformation in the intermediate region. In addition, the slower the diffusion processes proceeding the lower the temperatures at which the structural constituents are formed.

In low-carbon welds the similar effect is manifested by metal alloying with a complex of elements decreasing the coefficient of carbon diffusion [16], that promotes the suppression of decomposition of

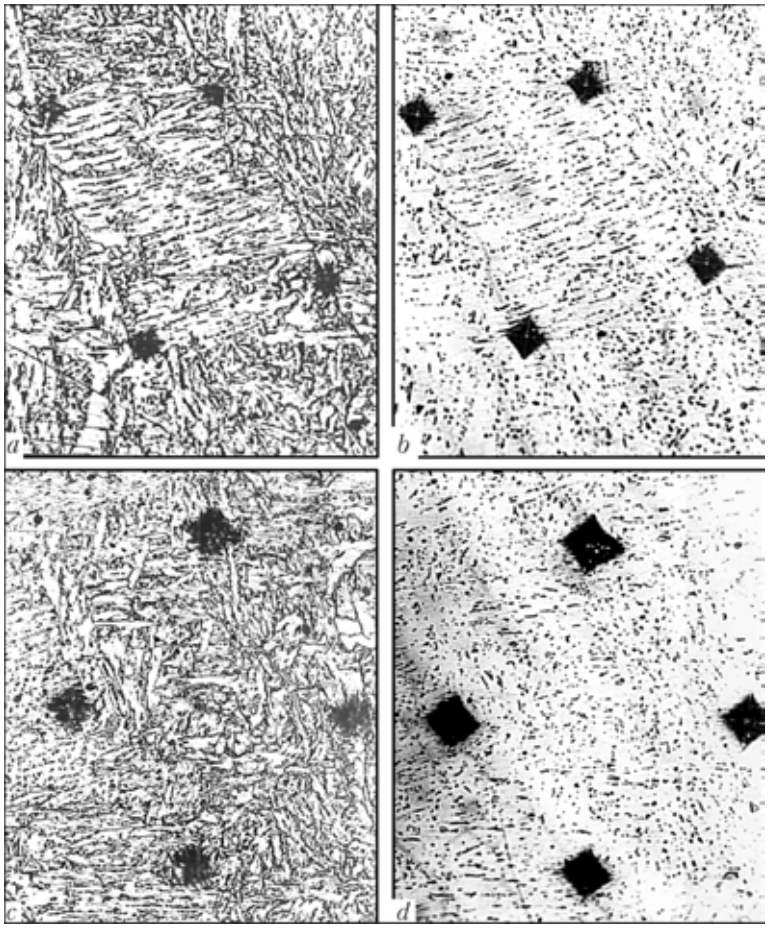

Figure 4. Microstructure of weld metal with MAC-phase in ferrite and ordered (*a*, *b*) and disordered (*c*, *d*) distribution of second phase (×500): *a*, *c* ---- etching in nithal; *b*, *d* ---- the same, in sodium picrate

residual austenite and shifting the final stage of its transformation to the region of temperatures at which such structures as AF and MAC-phase are formed. Comparison of data given in Tables 1 and 2, makes it possible to assume that effect of alloying elements on the conditions of formation of microstructures is the same in metal of welds with ULCC as in the low-carbon weld metal.

In metal of welds investigated the formation of the above-mentioned structures occurred in the region of temperatures of intermediate transformation and lower. It should be noted that the metal of low-alloy welds is not typical of the formation of carbides directly from austenite due to decreased temperatures of proceeding the austenite decomposition and low content of carbon. In this case the energetically more favourable process of enrichment of residual austenite with carbon is realized more intensively, which does not require such distinct differentiation of the mentioned element as in case of carbide precipitation. To prevent this process in weld metal, the content of those alloying elements which can intensify the liquation of carbon, for example silicon, should be minimized.

To check this assumption, the content of alloying elements in ferrite of different forms was determined (Table 3). Analysis of results obtained showed that the content of silicon and molybdenum in MF is higher than in PF or AF.

Silicon, decreasing the thermodynamic activity of iron, promotes the more intensive enrichment of local volumes of austenite with carbon. Coming from this, the silicon content in weld metal with ULCC should be reduced to minimum, to the level of not less than 0.3 wt.%, that will contribute to the suppression of the process of non-uniform distribution of carbon in solid solution and decelerate the process of formation of PF and MF.

Separate effect of MF on strength and ductile properties was not studied as its content in metal of welds is very negligible. Taking into account that with increase of a size of constituents of microstructure the characteristics of strength and toughness are decreased (Zinger's equation), we shall come to the following conclusion: MF is, probably, undesirable element of structure and can be the cause of instability of properties of low-carbon steels at low temperatures.

Coming from the fact that MF is enriched with silicon and molybdenum (see Table 3) it can be assumed that this form of microstructure was formed in the high-temperature zone of curve of austenite decomposition directly after the PF formation. However, this problem requires the further study.

Let us dwell separately on the peculiarities of MAC-phase formation in steels with ULCC.

For this purpose, special metallographic examinations of structure of metal in strictly fixed places of samples of weld metal with two levels of carbon content, 0.025 and 0.037 wt.%, were made. Here, the regions of MAC-phase with ordered and disordered second phase were selected (Figure 4).

The prepared samples were subjected to a successive etching in nithal firstly for revealing the secondary structure, and then in sodium picrate after the mechanical repolishing for revealing the MAC-phase. Analysis of microstructure was made by the comparison of images obtained. It showed that topography of distribution of MAC-phase in structure remains similar independently of carbon content in weld metal.

In structure with the ordered second phase the MAC-phase is located mainly in crystallographic planes of ferrite. However, the decreased content and higher dispersity of its component is typical of metal with ULCC. Its laminas, forming the oriented structure of ferrite with ordered second phase, are located at some distance from each other which is determined, probably, by the temperature of transformation. The obtained images allowed us to state that the thickness of elongated precipitations of MAC-phase is 1–3 μm.

Figure 5. Microstructure of low-alloy (*a*) and with ULCC (*b*) weld metal with MAC-phase (×1000)

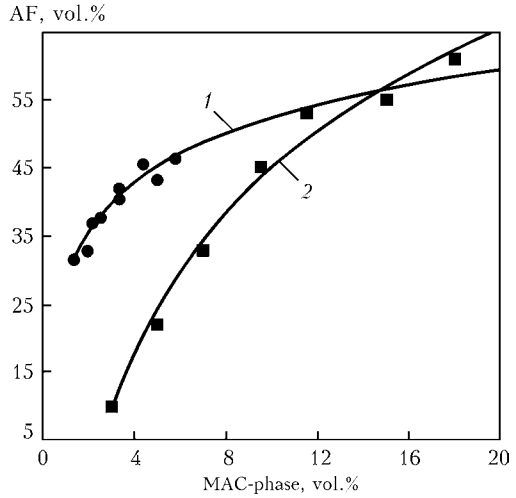

Figure 6. Interrelation between the AF content and MAC-phase in structure of weld metal: *1* — Al + Ti; *2* — Ni + Mn + Mo

MAC-phase in the structure with disordered second phase is located chaotically among the interlaced laminas of ferrite. Many precipitations of MAC-phase are blocked in microvolumes between the ferrite laminas having different orientation (Figure 5). Moreover, it was noted that the more narrow the ferrite laminas the thicker interlaminar precipitations of MAC-phase.

It is known that the thickness of ferrite laminas with different orientation depends on temperature and degree of austenite overcooling in weld metal, that defines the change in a shape of precipitating MAC-phase, i.e. from large (elongated) laminas to round particles, at decrease of temperature of residual austenite decomposition. These are the factors that defined the scattering in sizes and shapes of MAC-phase, precipitating in weld metal with ULCC and ordinary content of carbon (see Figure 5).

In connection with the fact that AF and MAC-phase are formed in places with the highest content of carbon in lower temperature region of intermediate transformation, we have made an assumption that interrelation may exist between the content of these two structural constituents of weld metal. It was observed in comparison of obtained secondary microstructure with a nature of MAC-phase distribution that its formation can occur in weld with ULCC without AF formation. Nevertheless, it is the latter that accompanies the MAC-phase formation in metal of many welds. It was found in conductance of investigations that the increase in AF content in structure of weld metal with ULCC is accompanied by the increase in amount of MAC-phase (Figure 6). The results obtained were checked on steel 10XSND welded joints, made with a low-alloy wire of a pearlitic class, alloyed with nickel, manganese, molybdenum, and also with wire Sv-04N3GTA under the agglomerated flux, into which aluminium and titanium were added additionally.

CONCLUSIONS

1. Main morphological forms of ferrite, forming in weld metal with ULCC, are defined.

2. Unlike the low-carbon weld metal, two more massive intragrain and near-boundary forms of ferrite, which have in definite cases either dendritic or disorientated form, are contained additionally in metal structure with ULCC.

3. Massive laminar formations, growing normal to the boundary of grains, can be referred to Widmanstatten type, though their appearance is differed from that of classic type.

4. To prevent the lamination of solid solution of austenite in carbon and deceleration of process of PF formation the content of silicon in weld metal with ULCC should be reduced to the level of lower than 0.3 wt.%, and the selected system of weld alloying should contribute to shifting the austenite decomposition to the region of intermediate transformations and lower. Owing to the latter it is possible to provide the maximum possible volume share of AF in the weld metal and to reduce the share of PF to minimum.

1. Irving, B. (1995) Steel companies emphasize improving weldability of HSLA steels. *Welding J.*, **4**, 39–44.
2. Morrison, W.B. (2000) Past and future development of HSLA steels. In: *Proc. of 4th Int. HSLA'2000 Conf. of High-Strength Low-Alloy Steels*, Xi'an, China, Oct. 30–Nov. 2, 2000.
3. Sato, A. (2000) Research project of structural materials for the 21st century (ultra-steels). *Ibid.*
4. Hrivnyak, I., Matsuda, F. (1994) Metallographic examination of martensite-austenite constituent (MAC) of HAZ metal of high-strength low-alloy steels. *Avtomatich. Svarka*, **3**, 22–30.
5. Okada, H., Matsuda, F., Ikuchi, K. et al. (1994) Decomposition behavior of M-A constituent and recovery of toughness. *Q. J. JWS*, **3**, 398–403.
6. Matsuda, F. (1990) An investigation on the behavior of M-A constituent in simulated HAZ of HSLA steels. *Doc. IIW IX-B-1591–90*.
7. Makara, A.M., Grabin, V.F., Denisenko, A.V. et al. (1967) About structural constituents of weld metal on low-alloy steels. *Avtomatich. Svarka*, **3**, 1–6.
8. Malinochka, Ya.,N., Pavlova, S.D., Slinko, L.A. (1966) Structure and properties of pipe welded joints from low-alloy steels. *Ibid.*, **4**, 13–17.
9. Grabin, V.F., Denisenko, A.V. (1978) *Metals science of welding of low- and medium-alloy steels.* Kiev: Naukova Dumka.
10. Josefsson, B., Andren, H.O. (1989) Microstructure and thermodynamic behaviour of a CrMo SA weld metal in as-welded state. In: *Proc. of Int. Conf. on Recent Trends in Welding Science and Technology*, Gatlinburg, May 14–18, 1989.
11. Duren, C. (1986) Formulas for calculating maximum hardness in the HAZ of welded joints. *IIW Doc. IX-1437–86*.
12. Yurioka, N. (1987) Prediction of HAZ hardness of transformable steels. *Metal Construction*, **4**, 271.
13. Rehmggan, A., Edmonds, D.V. (2000) Ferrite morphologies in ultralow carbon manganese steels. In: *Proc. of 4th Int. HSLA'2000* Conf. on High-Strength Low-Alloy Steels, Xi'an, China, Oct. 30–Nov. 2, 2000.
14. Popov, A.A. (1963) *Phase transformations in metallic alloys*. Moscow: Metallurgizdat.
15. Gulyaev, A.P. (1977) *Metals science*. Moscow: Metallurgizdat.
16. Vyaznikov, N.F. (1951) *Alloyed steel.* Moscow: Metallurgizdat.

ESTIMATION OF FORCES AFFECTING THE SPRAY METAL IN ELECTRIC ARC METALLISING

Yu.S. KOROBOV
The Urals State Technical University, Ekaterinburg, Russian Federation

Causes of difficulties underlying formation of a concentrated flow of spray material in electric arc metallising are considered. It is assumed that detachment of a large-diameter drop from the electrode tip under the effect of gas-dynamic pressure and its tear into smaller droplets under the impact of electromagnetic and gas-dynamic forces occur simultaneously in the arc. As shown by the estimations performed, forces of an electromagnetic nature have a magnitude similar to that of the aerodynamic ones. However, they differ in direction. Their level and direction satisfactorily explain the possibility of formation of fine droplets. In addition, the calculation data show that designing of a nozzle assembly of the electric arc metallising unit requires that special measures be taken to prevent scatter of droplets from the jet axis.

Keywords: *electric arc metallising, spray material, finely dispersed components, gas-dynamic pressure, electromagnetic forces*

Despite the fact that costs incurred in deposition of coatings by the electric arc metallising (EAM) method are 3–10 times as low as those characteristic of other thermal spraying methods [1], progress in this area is hindered by difficulties in forming a concentrated flow of a spray material. In turn, this leads to decrease in the material utilisation factor and quality of a coating. To reveal causes of the above problems, consider processes occurring in the arc zone during EAM (Figure 1).

It is concluded in studies [2, 3] that the dominant force among the forces that affect molten metal during the EAM process is the gas-dynamic one. Noted also is the effect of the electromagnetic forces, although with no estimation. Tear of droplets detached from the electrode tips into smaller ones is attributed to their secondary gas-dynamic splitting in flight. Calculations based on the diagram of critical size of the droplets, according to which the tearing forces are higher than the surface tension force, are made from the critical Weber number using the relationships of surface tension and relative velocities of gas and droplets characteristic of EAM. As shown by analysis of literature data [2, 4, 5] and our experimental results [6], the droplets detached from the electrode tips have weight similar to that of the droplets (for steel) with a diameter of 500–800 μm at a detachment interval of $(5–8)\cdot10^{-4}$ s. At a working distance, their diameter is equal to 10–300 μm. The content of the droplets with a diameter of less than 140 μm in a jet is 60–80 wt.%. These data disagree with those for calculated critical diameters d_{cr} of the droplets in EAM [3] (Al ---- 80, Zn ---- 72, Fe ---- 156, Ni ---- 180 and Cu ---- 118 μm), according to which no finely dispersed droplets with a diameter of 156 μm can be formed, e.g. for iron.

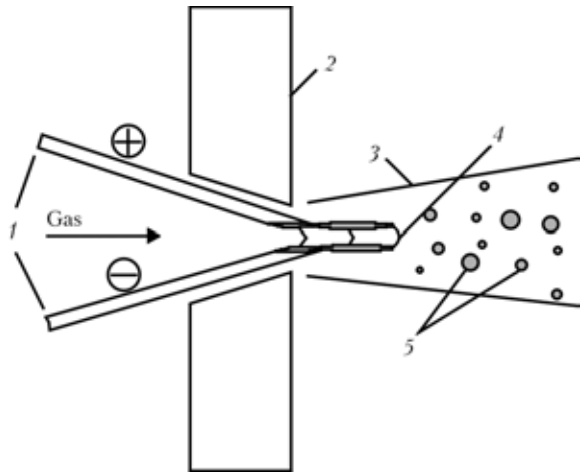

Figure 1. Flow diagram of the electric arc metallising process: *1* — wires; *2* — nozzle; *3* — gas jet; *4* — arc; *5* ---- molten particles

To explain formation of a finely dispersed component of the droplets, in collaboration with V.N. Boronenkov [6] we suggested the mechanism of formation of the droplets in the arc zone, other than that put forward in studies [2, 3]. It is assumed that detachment of a large-diameter drop from the electrode tip under the effect of gas-dynamic pressure and its tear into smaller droplets under the impact of electromagnetic and gas-dynamic forces occur simultaneously in the arc.

The following flow diagram is suggested for occurrence of this process (Figure 2). Affected by the gas-dynamic pressure, the molten metal is blown off from the electrode tip. With this it extends into a flat jet, i.e. tongue, held at the tip by the surface

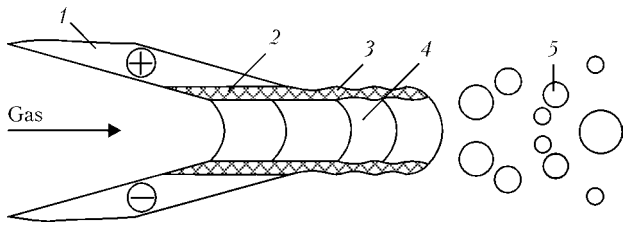

Figure 2. Diagram of detachment of droplets from the electrode tip in EAM: *1* — electrode; *2* — liquid interlayer; *3* ---- tongue; *4* — arc; *5* ---- droplets

© Yu.S. KOROBOV, 2004

tension forces. In accordance with the classical diagram by V.G. Levich [7], tear of the molten metal jet by the gas flow occurs in the neckings formed under the effect of gas pressure gradients in the zones of local disturbances. The current flowing through the tongue and the electric arc supplement this mechanism with the other, stronger mechanism of fracture of bridges [8]. Release of the Joulean heat in the neckings is more intensive than in the other regions of the conductor due to increased ohmic resistance. Therefore, metal and gas near the bridges are heated to higher temperatures. The combined processes of boiling of the molten metal and impact expansion of gas near the neckings result in further fracture of the jet.

In addition, electromagnetic forces are formed in the arc zone as a result of interaction of the current and induction flows. Studies [9, 10] describe interaction between the molten metal and electric arc for the case of arc welding (AW). However, this description is inapplicable to EAM, as the latter is characterised by the presence of a high-velocity gas flow and a special relative location of the cathode and anode, which dramatically changes parameters of the processes at the electrode tips. In particular, in EAM the size of the droplets is smaller and time of their detachment from the electrode tips is shorter by 1–2 orders of magnitude, compared with AW, and the direction and level of impact of the gas flow on the electric arc change. In AW the gas flow is directed along the electrode axis, whereas in EAM directions of the gas flow and electrode axes form an angle of 15–30°. The mean mass flow of gas in EAM is higher by a factor of 100. The inclined relative location of electrodes causes a sort of interaction of the magnetic and electric fields of the current flow.

Consider the effect of electromagnetic forces in the arc zone. Diagram of movement of the arc blown about by a transverse gas flow in a gap between the electrodes, as suggested in study [11], is confirmed by the data of high-speed filming. According to this diagram, where the transverse gas flow affects the arc, the arc column retains its cylindrical shape, while the plasma flows attached to the reference spots are blown off under the combined effect of the Ampere force and gas-dynamic pressure.

However, in the case of EAM, correctness of the assumption that the arc column has a cylindrical shape and its axis is normal to the electrode tips requires an additional estimation because of a high velocity of the gas jet blowing about the electrode tips. Calculate velocities of the arc and gas-plasma flows blowing about it.

The arc column is contracted due to the pinch effect, i.e. interaction of the current flowing in the column with its natural magnetic field. This results in a longitudinal pressure gradient. In turn, it induces the plasma flows from the regions of the reduced section. According to the Bernoulli law, for this case the maximal velocity of plasma in a flow can be determined from the equation given in [11]:

$$v_{pl} = \sqrt{(\mu I j)/(2\pi\rho_g)}, \qquad (1)$$

where μ is the magnetic permeability of a medium corresponding to vacuum, H / m; $I = \pi r^2 j$ is the arc current, A; j is the current density, A / m^2; ρ_g is the gas density, kg / m^3; and r is the arc column radius, m.

If we assume that radius of the arc column is equal to that of the electrode, for typical conditions (I = = 200 A) this will correspond to $j = 6.4 \cdot 10^7$ A / m^2. According to equation (1), velocity of the plasma flow, v_{pl}, under the above conditions is 140 m / s. These calculation results are close to the experimental data obtained from the filmograms of movement of the probe droplet [10]. This value of v_{pl} is in a range between the velocity of the plasma flow in the arc column in AW (v_{pl} = 78 m / s, where $j = 2 \cdot 10^7$ A / m^2 [9]) and that of the plasma flow in a plasmatron (v_{pl} = 393 m / s, where $j = 5 \cdot 10^8$ A / m^2 [12]).

Velocity of the arc in a gap between the electrodes can be estimated from the frequency of detachments of droplets, this following from the physical notion of the mechanism of arc formation between the electrode tips. First the arc shunting takes place in a region that is most favourable in terms of energy, i.e. at the internal edges of the tips. Then the arc moves to the leading edges of the tips. Here the arc column bends and its length increases. The difference of potentials between the cathode and anode remaining unchanged, this leads to extinction of the arc. Then the process again begins with the arc shunting at the internal edges. At an electrode diameter of 2 mm, its angle of inclination to the central axis equal to 15° and a characteristic detachment interval of $5.7 \cdot 10^{-4}$ s, velocity of the arc column is

$$v_{a.c} = 2 \cdot 10^{-3} / (\sin 15° \cdot 5.7 \cdot 10^{-4}) \approx 12 \text{ [m / s]}. \qquad (2)$$

Velocity of gas in a gap between the electrodes is determined from thickness of a molten interlayer blown off by the gas flow from the electrode tip. Dependence of thickness of the viscous layer, δ, carried away by the gas flow upon the velocity of gas and properties of the molten metal [7] was derived from the Newton equation for a case of flow of thin films of fluids:

$$\delta = (\sigma \nu / \rho_p v_g^3)^{0.5}, \qquad (3)$$

where ρ_p, σ and ν are the density (kg / m^3), surface tension (J / m^2) and kinematic viscosity (m^2 / s) of molten metal; and v_g is the velocity of gas in a gap at the external boundary of the interface layer (m / s). Express the velocity of gas in the gap through expression (3):

$$v_g = (\sigma \nu / \rho_p \delta^2)^{1/3}. \qquad (4)$$

It is assumed in the calculations that σ = 1.5 J / m^2 [13] for molten metal temperature T = 2500 K.

Thickness of the interlayer carried away by the gas flow is estimated from the condition of equality of volume of the detached interlayer and that of the

droplet, according to the data of oscillography of detachment of droplets in EAM [2, 4]. For a characteristic detachment interval of $5.74 \cdot 10^{-4}$ s, the mass of a droplet, m, is $6.4 \cdot 10^{-7}$ kg. If we assume that thickness of the detached interlayer is uniform over the electrode tip, it will be equal to

$$\delta = m/(\rho_p S_s) = 6.4 \cdot 10^{-6} \ \text{[m]}, \quad (5)$$

where S_s is the surface area of the electrode tip, m^2. Calculation of the velocity of gas in the gap from equation (4) yields $v_g \sim 1.5$ m / s.

To evaluate correctness of the calculation, compare thickness of the detached liquid interlayer with that of the molten metal layer at the electrode tip. For this, use the following form of the equation of heat balance of an electrode:

$$Q_e = Q_c + Q_{sp} - Q_{con}, \quad (6)$$

where Q_e is the total heat received by the electrode; Q_c is the heat released in the electrode due to the current flow; Q_{sp} is the heat released due to active spots of the electric arc; and Q_{con} are the convective heat losses. Expand this equation as follows:

$$c\gamma v_f \frac{dT}{dL} = j^2\rho + \frac{c\gamma v_f (T_d - T)}{L - L_x} \exp\left(-c\gamma v_f (L - L_x)/\lambda\right) - 4\alpha_{tr}(T - T_g)/d, \quad (7)$$

where ρ is the specific electrical resistance, Ohm·m; γ is the density of the solid electrode material, kg / m^3; v_f is the wire feed speed, m / s; L is the electrode extension, m; L_x is the current value of the electrode extension, m; T and T_d are the temperatures of the droplet (current value and at the electrode tip, respectively), K; T_g is the gas temperature, K; λ is the coefficient of thermal conductivity of the metal droplet, W / (m·K); α_{tr} is the coefficient of surface heat transfer calculated from the Nusselt number, W / (m^2·K); and d is the electrode diameter, m.

Heating of the electrode from active spots of the arc, Q_{sp} (due to rapid heat input) was calculated using the equation of propagation of heat from a continuous-action flat source in a rod, which moves at a constant speed. Temperature dependencies of specific electrical resistance ρ and specific metal heat c were approximated by equations of the form of $y = a1T^2 + a2T + a3$, according to studies [14, 15].

As shown by numerical calculations from equation (7), made for the input data typical for EAM, thickness of the liquid interlayer at the tip is $11 \cdot 10^{-6}$ m. An additional calculation of thickness of the molten metal layer was made for the same input data. This calculation was made in accordance with solution of the problem of melting of a cold body having a limited size with a continuous removal of the formed melt, allowing for the enthalpy of melting [16]. The resulting thickness of the molten metal layer is $7.6 \cdot 10^{-6}$ m. Relationship of this value according to both calculations and thickness of the liquid interlayer corresponds to the qualitative picture of the process, where part of the molten metal layer is blown off by the gas flow.

Table 1. Velocities in the gap

Velocity	*Calculation equation*	*Value, m/s*
v_{pl} (plasma flowing about the arc column)	(1)	140
$v_{a.c}$ (arc column moving over the tips)	(2)	12
v_g (transportation gas in the gap)	(4)	1.5

The calculation results on the velocities of the arc column, as well as gas and plasma flows in the gap between the electrode tips are given in Table 1. As follows from the Table, velocity of the transportation gas flow is low compared with that of plasma in the arc and column in the gap. Therefore, it can be concluded that the arc column most probably has the cylindrical shape with an axis normal to the gas flow, and its movement occurs mainly due to the electromagnetic forces.

Estimate the level and direction of forces affecting the necking in the tongue detaching from the electrode tip. If we assume that the mutual pressure of metal vapours from both tips is balanced, it seems to be affected by the following forces (Figure 3):

- $F_{a.r}$ (aerodynamic resistance);
- F_f (pressure at the shock wave front in explosion-like expansion of metal vapours and gas near the necking);
- Ampere force F_1 (interaction of the magnetic field of the electrode extension and current in the necking);
- Ampere force F_2 (pinch effect);
- Ampere force F_3 (interaction of the magnetic field of the arc column and current in the necking).

The force of aerodynamic resistance, $F_{a.r}$, can be calculated as follows:

$$F_{a.r} = 0.5 C_{a.r} S \rho_g (v_g - v_p)^2, \quad (8)$$

where $C_{a.r}$ is the coefficient of aerodynamic resistance; $S = \pi d_b^2 / 4$ is the surface of the midlength section, m^2; v_g and v_p are, respectively, the velocities of gas and particles, m / s; and d_b is the bridge diameter, m.

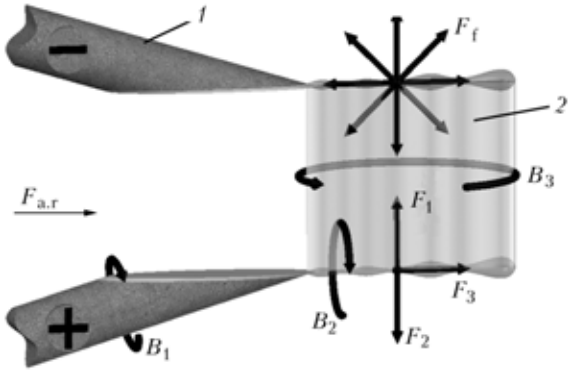

Figure 3. Schematic of forces in the arc zone: *1* — electrode; *2* — arc column

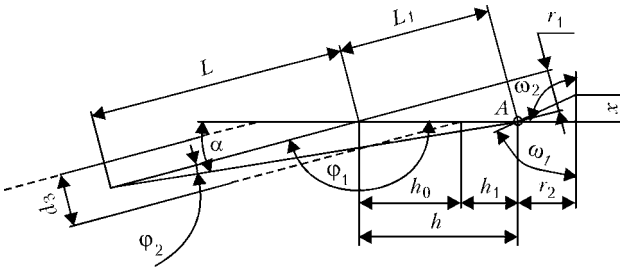

Figure 4. Diagram for the calculation of electromagnetic forces in the arc zone

The value of F_f due to the pressure at the shock wave front, P_f, on the surface of the necking with radius r_n and length Δh is

$$F_f = P_f 2\pi r_n \Delta h. \quad (9)$$

According to the mechanism of tear of the tongue, as we suggested, the current flowing through the neckings dramatically enhances the heat released in them, which is caused by an increased ohmic resistance. This initiates tear of the tongue in the neckings and, hence, formation of microacrs in the tear regions, thus leading to an explosion-like expansion of metal vapours and gas. The expansion of gas causes a dramatic increase in its volume and propagation of a shock wave, accompanied by the energy release. Pressure at the shock wave front can be expressed through the following relationship [17]:

$$P_f = \frac{2\gamma_g^0}{\kappa + 1} v_{fr}^2, \quad (10)$$

where γ_g^0 is the initial density of gas, kg / m^3; κ is the adiabatic constant; and v_{fr} is the velocity of the front of an expanding gas, m / s.

Velocity v_{fr} can be estimated from the equality of forces of the gas-dynamic pressure and capillary pressure in the bridge preventing its fracture [8]:

$$v_{fr} = \sqrt{\frac{16 C_{a.r} \sigma}{d_b \gamma_g}} = 1520 \ \ [\text{m / s}]. \quad (11)$$

Diameter of the bridge, d_b, is assumed to be equal to thickness of the blown off layer, δ, as estimated from equation (5).

In addition to the gas-dynamic forces, the bridge is affected also by the electromagnetic forces caused by the current flowing through the tongue and electrodes. Three main directions can be distinguished in the current flow relative to the axis of the gas flow (Figure 3):

- current flow along the electrode extension with length L at angle α;
- current flow over the molten metal layer;
- current flow along the arc column with length x.

Magnetic induction B_1 of the electrode extension at the central point of necking, A, can be calculated from the equation of the magnetic field of a straight-line conductor [13]:

$$B_1 = \frac{\mu I}{4\pi r_1} (\cos \varphi_2 - \cos \varphi_1). \quad (12)$$

According to the diagram shown in Figure 4, r_1 is the shortest distance from point A to the electrode axis; and φ_1 and φ_2 are the angles between the vector of current density in the conductor and radius vectors drawn to point A from the beginning and end of the conductor, respectively. Angles φ_1 and φ_2 are determined by the angle of inclination of the electrode, α:

$$\cos \varphi_1 = \cos(180 - \alpha) = -\cos \alpha; \quad r_1 = h \sin \alpha; \quad (13)$$

$$\cos \varphi_2 = L + h \cos \alpha / \sqrt{(h \sin \alpha)^2 + (L + h \cos \alpha)^2}, \quad (14)$$

where $h = d_e / 2\sin \alpha + h_1$.

The necking Δh long is affected by force F_1 induced by interaction of the magnetic field (induction B_1) and current flowing through the necking:

$$F_1 = I B_1 \Delta h. \quad (15)$$

Local reduction of the conductor in the necking results in formation of force F_2 induced by the pinch effect. The pinch effect is caused by interaction of the current flow and magnetic field (induction B_2):

$$F_2 = \mu I^2 \ln(r_{\tilde{n}} / r_n) / 4\pi. \quad (16)$$

In analogy with equation (12), the numerical value of magnetic induction B_3 at point A is

$$B_3 = \mu I(\cos \omega_2 - \cos \omega_1)/(4\pi r_2) = \mu I(1 - x / h_2)/4\pi h_2, \quad (17)$$

where $\omega_2 = 90°$, according to the assumption that the arc column is normal to axis of the gas flow. Interaction of the magnetic field of the arc column with current in the necking yields force F_3:

$$F_3 = I B_3 \Delta h. \quad (18)$$

Results of the calculations of forces blowing off droplets from the electrode tips are given in Table 2.

The following assumptions were made in the calculations. The tongue is split into identical droplets with a diameter of $100 \cdot 10^{-6}$ m, thickness of the tongue is $7 \cdot 10^{-6}$ m; $\mu = 4 \cdot 10^7$ H / m; $v_g = 300$ m / s; and $\Delta h = 1 \cdot 10^{-6}$ m.

The calculation results given in Table 2 are of an estimation character, which is attributable to shortage

Table 2. Calculation of forces in the arc zone affecting the molten metal

Force	*Equation*	*Value, $\cdot 10^5$ N*
$F_{a.r}$ (aerodynamic resistance)	(8)	7.1
F_f (shock wave pressure)	(9)	5.6
Ampere force F_1 (electrode extension magnetic field – current in necking)	(15)	5.2
Ampere force F_2 (pinch effect)	(16)	9.4
Ampere force F_3 (arc column magnetic field – current in necking)	(18)	0.03

of the experimental data. Nevertheless, the calculations show that forces of the electromagnetic nature are of the same magnitude as the aerodynamic force, but differ in direction from the desirable one for movement of the droplets. Therefore, our assumption of the probability of tear of the droplets in the arc zone under the effect of not only the aerodynamic but also electrodynamic forces is valid to a sufficient degree.

CONCLUSIONS

1. The level and direction of forces in the arc zone provide a satisfactory explanation to the possibility of producing small-diameter droplets.

2. Designing of the nozzle assembly of the electric arc metallising unit requires that special measures be taken to prevent scatter of the droplets from the jet axis.

1. Kharlamov, Yu.A. (2000) Flame spraying of coatings and environmental safety of manufacture, repair and service of machines. *Tyazh. Mashinostroenie*, **2**, 10–13.
2. Vakhalin, V.A., Maslenkov, S.B., Kudinov, V.V. et al. (1981) Process of melting and spraying of electrode material in electric arc metallising. *Fizika i Khimiya Obrab. Materialov*, **3**, 58–63.
3. Ageev, V.A., Belashchenko, V.E., Feldman, I.E (1989) Analysis of methods for controlling parameters of spray particles in arc metallising. *Svarochn. Proizvodstvo*, **12**, 30–32.
4. Krechmar, E. (1966) *Deposition of metals, ceramics and plastics.* Moscow: Mashinostroenie.
5. Gubenko, B.G., Borisova, A.L., Kostin, V.A. et al. (1990) Structural heterogeneity of electrometallised coatings of 65G steel. *Avtomatich. Svarka*, **6**, 19–23.
6. Korobov, Yu.S., Boronenkov, V.N. (2003) Kinetics of interaction of spray metal with oxygen during electric arc metallising. *Svarochn. Proizvodstvo*, **7**, 30–36.
7. Levich, V.G. (1959) *Physical-chemical hydrodynamics.* Moscow: Fizmatgiz.
8. Shejkhaliev, Sh.M. (1977) *Investigation of splitting of metal jets by electric current.* Syn. of Thesis for Cand. of Techn. Sci. Degree. Sverdlovsk.
9. Leskov, G.I. (1970) *Electric welding arc*. Moscow: Mashinostroenie.
10. Lenivkin, V.A., Dyurgerov, N.G., Sagirov, Kh.N. (1989) *Operational properties of gas-shielded welding arc*. Moscow: Mashinostroenie.
11. Bron, O.B., Sushkov, L.K. (1975) *Plasma flows in electric arc of switching-off units.* Leningrad: Energiya.
12. Zhukov, M.F., Smolyakov, V.Ya., Uryukov, B.A. (1977) *Electric-arc gas heaters (plasmatrons)*. Moscow: Nauka.
13. Yavorsky, B.M., Detlaf, A.A. (1985) *Refer. book on physics*. Moscow: Nauka.
14. Asnis, A.E., Gutman, L.M., Poklady, V.R. et al. (1982) *Welding in active gas mixture*. Kiev: Naukova Dumka.
15. Elliot, F., Gleiser, M., Ramakrishna, V. (1969) *Thermochemistry of steelmaking processes.* Moscow: Metallurgiya.
16. Goldfarb, E.M. (1967) *Heat engineering of metallurgical processes.* Moscow: Metallurgiya.
17. (1978) *Pulsed light sources*. Ed. by I.S. Marshak. Moscow: Energiya.

SPECIFICS OF ARC SPOT SHIELDED-GAS WELDING PROCESSES (REVIEW)

N.M. VOROPAJ
E.O. Paton Electric Welding Institute, NASU, Kiev, Ukraine

Peculiarities of processes of arc spot consumable and non-consumable electrode welding of carbon and alloyed steels, non-ferrous metals and alloys are considered. Parameters of welding in active and inert gases and also the mechanical properties of overlap joints made by the given method are presented. Prospects of development of arc spot welding technology are outlined.

Keywords: *arc welding, consumable electrode, pulsed-arc welding, non-consumable electrode, spot welded joints, CO_2, argon, mixture of gases, synergic control, welding technology*

Arc welding in shielding gases has found the wide spreading in manufacture of structures from carbon and alloyed steels, non-ferrous metals and alloys [1]. Important trends for the further improvement of the arc welding are the programming of electrode wire feed speed by the laws providing a forced transfer of drops [2, 3]; separate feeding of current pulses to two electrodes isolated one from another [4, 5]; pulsed-arc welding with a synergic control of condition parameters [6], and also hybrid technologies of plasma and arc welding [7]. The latter include five processes: plasma-MIG, plasma-TIG, welding with opposite arc and plasma, welding with heteropolar current pulses and plasma-arc «Hydra-process».

Undoubted advantage of the shielded-gas arc welding is the feasibility to produce the quality overlap joints welded by separate spots (rivet welds) [1, 8]. The main types, design elements and sizes of spot welded joints from different metals and alloys are regulated by GOST 14776–80 [9]. In this case the following terminology and designation of welding processes are accepted: with consumable electrode in CO_2, with consumable electrode in inert gas, with non-consumable electrode in inert gas, with forced formation, on a removal backing and with a forced penetration. Information about automatic arc spot welding, procedures of stud welding and spot hardfacing are generalized in work [8].

The experimental data gained about the electric and heat characteristics of arcs allowed us to use the calculation methods for determination of optimum conditions of arc spot welding, which give a desired shape and sizes of the penetration zone and the most favourable thermal cycle. The insufficient heating of parent metal leads to lack of penetration, abruptly reducing the strength of the welded joint. Excessive heating causes the through penetration of the product, and also noticeable phase and structural changes in weld metal and HAZ.

© N.M. VOROPAJ, 2004

To study the dependence of change in penetration shape on the spot welding conditions, the calculation graphs of penetration depth h depending on arc power q and duration of welding t_w of sheets of various thickness were constructed [8]. In the period of heat saturation the depth of penetration is proportional to the amount of heat, generated in the product, i.e. q and t_w. At welding time of less than 2 s the depth of penetration is changed negligibly.

The expediency of CO_2 use as a shielding gas in arc spot welding of steel metal structures was grounded in work [10]. In the opinion of authors, the advantages of this method over the submerged arc welding consist in a larger depth of penetration of rivet welds, low susceptibility to rust and absence of inconveniences connected with flux and slag feeding and cleaning. The best results were obtained in CO_2 welding with wire Sv-10GS of 1.6–2.0 mm diameter. The favourable formation of heads of rivets was attained in welding under the voltage, being higher than that in conventional process of CO_2 welding (Table 1). With increase in arc voltage a pimple is formed in the center of deposit, while with decrease in arc voltage a depression is formed.

Analysis of published works shows that optimum is the shape of rivet welds which have the larger penetration depth h and smaller height of convexity g at preset diameters (upper D and lower d) (Figure 1). Coefficient of penetration shape k_p is equal to the ratio of penetration depth to head diameter ($k_p = h / D$), while the coefficient of head shape is $k_{sh} = g / D$. It was found that using the joint with rivets it is necessary to have a high coefficient of penetration shape and a low coefficient of head shape. In arc spot welding in CO_2 the rivets have the more favourable shape as compared with those in submerged arc welding. Strength properties of joints made in CO_2 are not inferior to those made by submerged arc welding.

In arc spot CO_2 welding of thin metal by electrode wire of 0.8–1.0 mm diameter the quality of rivet welds are defined by the stability of arc exciting [11]. The latter is improved with decrease in electrode stickout, increase in current density and rate of its increment at the short-circuit moment. Optimum conditions of

Table 1. CO_2 welding conditions and sizes of rivet welds

Thickness of metal welded, mm	*Welding condition*				*Sizes of rivet welds*		
	Electrode wire diameter, mm	*Welding current, A*	*Arc voltage, V*	*Time of welding, s*	*Diameter of head, mm*	*Height of convexity, mm*	*Depth of penetration, mm*
2 + 2	1.6	220	27–30	0.5	13.0	2.0	2.5
3 + 3	1.6	260	30–32	0.5	14.5	1.5	4.0
5 + 5	2.0	300	32–34	1.5	16.5	1.3	2.3
≥ 6	2.0	450	35–37	1.5	23.0	2.0	6.0

welding metal of 0.5–1.5 mm thickness provide a stable arc burning, minimum spattering of electrode metal and good weld formation. Sufficient penetration of the lower sheet is attained in the presence of hole in the upper sheet. The arc discharge is energized usually at a continuous electrode feeding to the product without the wire reverse or preliminary short-circuiting of the electrode.

Rivet welding is performed in all spatial positions. Electrode wire of 0.8–1.2 mm diameter is used for welding at current up to 300 A, while that of 1.6–2.0 mm diameter is used at current above 400 A. The thickness of upper sheet welded in these cases reaches 5–6 mm. When the electrode wire of 3–4 mm diameter and programming of welding condition parameters are used, the depth of penetration is increased up to 8–10 mm [12]. Cycle of arc spot welding is divided conditionally into the following technological stages:

- heating of surface of parts being welded in site of making spot weld;
- burn-through of upper part and penetration of lower part;
- welding-up of spot weld with filling of hole with a molten electrode metal;
- welding-up of spot weld crater providing excellent appearance of the welded joint.

The duration of each stage influences the quality and sizes of spot welds. If to weld-up the crater not for one stage, but for two stages, then the structure and appearance of welds is improved owing to the repeated heating. On this basis, a twin-electrode automatic machine A-1731, designed for welding sheets up to 6 mm thickness with spot welds to the bases of different flat structures, has been created. The automatic machine provides the pressing of parts and can be remote controlled.

In work [13] the resistance to corrosion fatigue of overlap joints. made by a resistance spot welding, using the automatic CO_2 welding with continuous welds and arc spot CO_2 welding, was determined. It was shown experimentally that joints produced by a bicycle arc spot CO_2 welding are characterized by the highest resistance against the corrosion fatigue. This method of welding is recommended for manufacture of components of railway cars and other panel structures.

Welding head for simultaneous CO_2 welding of two spots has been designed [14]. The distance between both torches is changed from 15 to 90 mm. The head is designed for welding products made from sheet material and from bars.

The experience of industrial application of arc spot welding showed that holes with a conical reaming are drilled for the thick upper sheets. The unique method of rivet welding was suggested in work [15]. Both stages of welding (penetration of sheets and crater filling) are proceeding automatically by the preset parameters. Rivet head is formed in a copper ring whose height defines the head reinforcement height. Thickness of metal welded reaches 30 mm.

The method of arc spot welding with consumable electrode in argon was used for aluminium alloys, not subjected to heat hardening [16]. The main obstacle in welding of aluminium alloys is the maintaining of weld pool metal from flowing out in case of a single-side access to the site of joint. To prevent the metal flowing out, it is necessary to limit strictly the time of arc burning. Finally, the strength of samples of overlap joints is defined by the cross-section area of spots in the zone of two sheets fusion.

At similar sizes of weld spots the strength depends also on the thickness of parts welded. In the process of welding heat-hardened alloys (for example, alloy VAD-1) the formation of crystalline cracks, causing the low strength of welded joints, is possible in rivet metal. In the near-weld zone of weld spots the structure of metal is not almost violated. With increase in

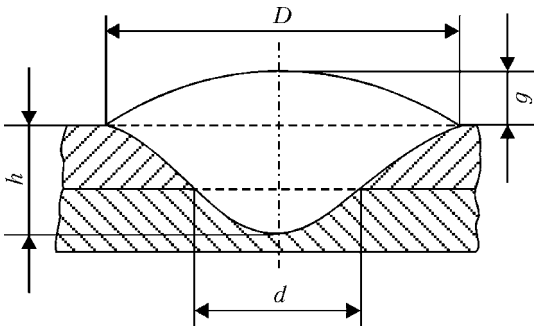

Figure 1. Scheme of a spot welded joint

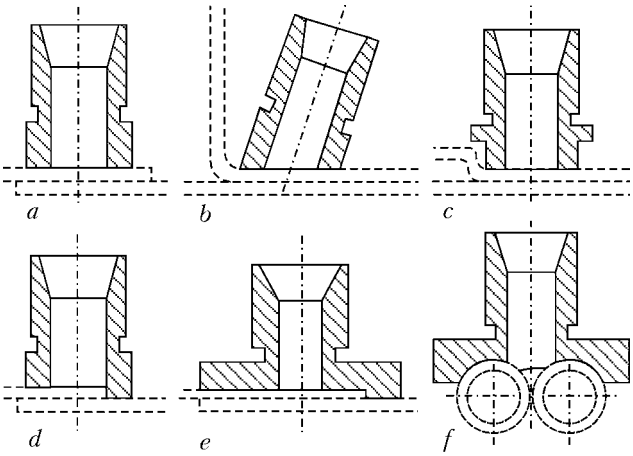

Figure 2. Schemes of cross-sections of nozzles for arc spot non-consumable electrode welding: *a* — standard; *b* — angular; *c* — with decreased diameter; *d* — with a control of a weld spot location from upper sheet edge; *e* — the same, but providing the pressing of upper sheet; *f* — tack welding of pipes located parallel

time of welding above 3 s a fine porosity was observed in the deposited metal. The decrease in welding time leads to the weld weakening, formation of discontinuities and porosity in a central part of the weld spots. Preliminary preparation of surface of parent metal and welding wire influence greatly the occurrence of these defects.

Arc spot welding with consumable electrode in argon and helium was performed for high-strength aluminium alloys of Al–Zn–Mg system [17]. Positive results were obtained only in use of the electrode wire of Sv-AK5, Sv-AMg5 grades. In non-consumable electrode welding the pores, hot cracks and unwelded craters of welds were observed.

In case of the consumable electrode welding the intensity of formation of these defects is lower and depends on condition parameters (welding current, arc voltage, consumption of shielding gas). With increase in current the depth of penetration is increased. At the same time the spot diameter is little changed.

The increase in arc voltage leads to the increase in spot diameter and to some decrease in depth of penetration. It was noted that the pores and hot cracks are observed more often in argon than in mixture of Ar + 70 % He or in mixture of Ar + 0.1 % N_2.

Specialized equipment for arc spot welding has been developed on the base of equipment for the mechanized consumable electrode welding [18]. It consists of a welding rectifier with a flat characteristic, a device for welding process control and a torch with special nozzles. The latter are used of two types: without and with water cooling.

The control diagram provides the preliminary supply of shielding gas and wire feeding, control of welding time and disconnection of wire feeding without nozzle fusion. Shielding gas is pure argon or mixture Ar + 1 % O_2 and Ar + 2 % CO_2. Welding in mixtures is performed at direct current (straight polarity) without drilling holes in the upper sheet. In CO_2 welding (reverse polarity) hole of 6–8 mm diameter is drilled in the upper sheet. Overlap spot welds are made on steels and aluminium alloys of about 3 mm thickness.

Technology of consumable electrode rivet welding of linings, made from alloy AMg6, to frameworks, made from pressed or stamped shaped sections, has been developed by the Rostov Institute of Agricultural Machine-Building, Russia [8]. Welding is performed by the electrode wire of Sv-AMg6 grade of 2 mm diameter in argon. A through penetration of elements welded was envisaged. Diameter of rivet head was 20–22 mm, height of convexity was about 2 mm. The head surface is smooth with a small shrinkage cavity in the center. Typical conditions of welding metal of thickness (1.2 + 3.5) mm was the following: welding current — 160 A; arc voltage — 22 V; welding time — 2 s.

Rivet welding was used for lining of refrigerator chambers with stainless steel. The following conditions for sheets of (1.8 + 2.8) mm thickness were recommended: wire diameter — 1.2 mm; welding current — 220 A; arc voltage — 28 V; welding time — 2.4 s.

Specifics of a pulsed-arc spot welding with consumable electrode in argon and helium, and also the properties of produced overlap joints from aluminium alloys of AMg6 and AD-33 grades were studied in work [19]. The preliminary drilling of holes in upper sheets provides the guaranteed penetration of the lower sheet and decrease in convexity of spot weld, significant increase in weld spot nugget and 20 % decrease in heat input to the parent metal.

The maximum effect was attained at a relatively high current and minimum time of welding. The spot welding was performed from power source «Fronius TPS-450», equipped with a special torch with a tip, providing a constant distance between the torch nozzle and upper sheet. Thickness of metal welded was 1.8 and 3.8 mm; diameter of wire Sv-AMg6 was 1.2 and 1.6 mm.

Frequency of pulses was 90–240 Hz, duration of current pulses was 2.5–3.5 ms. Replacement of argon by helium leads to 20–40 % increase in spot nugget diameter and 1.5–2 times increase in the metal penetration depth.

The comprehensive information about the technology of arc spot non-consumable electrode welding of alloyed steels is given in work [20]. Equipment for realization of this process consists of DC power source, controller of welding time and riveting device. The process can be applied to carbon, medium-alloy and stainless steels. Negative results were obtained in use of heat-resistant steels, copper and its alloys.

The quality of welded joints was improved by using a system of current reduction at the completion of spot weld formation. In case of the presence of a gap between the mating surfaces of parts the lower sheet is heated to a lower degree as compared to the upper sheet.

Similar peculiarities of arc spot non-consumable electrode welding were observed in use of Ar + He

mixture as a shielding gas [21]. Six varieties of nozzles for arc spot non-consumable electrode welding were studied (Figure 2). The sequence of welding operations in this case was as follows:

- a riveting device with an appropriate nozzle contacts the part welded;
- when pressing the button «Start» the tungsten electrode is fed to the product;
- the arc is excited and electrode is lifted upwards;
- welding is performed during 1–5 s.

Increase in welding duration promotes the increase in weld width (Table 2). Replacement of argon by helium leads to the increase in depth of penetration and decrease in weld width. The consumption of shielding gas has a little influence on the weld sizes. Strength characteristics of weld spots on killed and rimmed steels are little differed from each other. Diameter of weld spot from reverse side is not indicative for determination of the joint strength.

Formation of welds in the process of arc spot non-consumable electrode welding of aluminium alloys was studied at variation of current, composition of activating paste and shielding gas [22]. Current cycle consisted of heating, penetration and welding-up of crater. At the stage of heating the current of arc in helium was increased at a rate of 200–500 A / s and 1.5–2.0 mm arc length. The further penetration was performed by a short arc at unchanged current. Crater was welded-up at decreased current with a simultaneous elongation of arc. Paste, based on chlorine and fluoride salts of alkali metals, shifted the arc from the spot center to the periphery areas. Recommended condition of welding alloy AMg6 is the following: I_w = 180–210 A; t_w = 3.5–4.5 s.

The quality joints of thin-sheet aluminium alloys in arc spot welding in argon can be obtained by using the variable-polarity square shape current [23]. In this method of welding the oxide film is destroyed over the entire surface of the cast nugget. The moment of feeding the filler wire is coincided with the beginning of crater welding-up. The arc length in heating and melting of parent metal, the same as in the previous method, is 1.5–2.0 mm, while in crater welding-up it is 3–5 mm. The frequency of variable-polarity current in heating and melting is 6–8 Hz. In welding-up of crater it was increased up to 25–40 Hz.

To determine the rate of non-consumable immersion in arc spot welding, a probe, measuring the conductivity in near-electrode region of welding torch near the welding arc, is used [24].

Distance from the non-consumable electrode end to the surface of pool and its sizes were found experimentally. Programming of the cycle of arc spot welding using a probe provided a good weld formation and high level of mechanical properties of welded joints.

According to the article [25] it is possible to improve the process of formation of butt and overlap joints using a drop dosing of the filler metal. Detachment of molten drop and its deposition on the parts were realized in a forced way by increasing the rate of shielding gas flow. To provide the stability of the welding process the programmed change in arc current was used. At the beginning of the cycle the current of pilot arc was preset low and then it was increased up to the operating value. The welding was performed both without any backings and also on a removable backing.

Table 2. Conditions of argon arc rivet welding of carbon and stainless steels

Thickness of elements welded, mm		*Welding current, A*	*Time of arc burning, s*	*Nugget diameter, mm*
Upper	*Lower*			
0.5	0.5	40–50	0.5–0.8	3–4
	2.0	50–60	1.0–1.3	
0.8	0.8	80–90	1.5–1.8	4–5
	2.0	100–120	1.7–2.0	
1.2	1.2	110–120	1.7–2.0	5–6
	2.0	130–150	2.0–2.5	6–7
2.0	2.0	190–210	4.0–5.0	8–9

The positive results of single-sided arc spot non-consumable electrode welding on thin-sheet stainless steel SN-2 and titanium alloy OT4 were obtained in work [26]. The joint is formed as a result of a through penetration of the upper element by the arc burning in argon during 0.2 s. Thickness of the upper sheet was 0.4 mm, while that of the lower sheet was 0.6–15.0 mm.

A specialized installation, designed for these purposes, consisted of a casing, console, pneumatic cylinder, slide and welding head. The removal of craters in rivet weld was made by the second short-time pulse of current whose duration was equal to the duration of the first main pulse. All the cycle of the process of mechanized two-pulse welding consisted of the following operations:

- compression of elements welded;
- system blowing with argon;
- feeding of main welding pulse;
- feeding of auxiliary pulse (crater welding-up);
- holding of argon feeding for metal cooling.

Value of welding current was selected coming from the condition of obtaining required spot diameter and degree of penetration of the lower sheet. Excessive increase in current has led to the increase in diameter of molten zone and decrease in life of the tungsten electrode. In this case, a large shrinkage of spot metal was observed, the craters in welds, circular cracks and porosity appeared. It is typical that argon blowing from the reverse side of metal welded is required in welding of titanium alloy and stainless steel. With increase in time of welding the diameter of penetration zone is greatly increased, while the depth of penetration is little changed.

The Design Office of the E.O. Paton Electric Welding Institute has offered a small-sized device for electric arc spot welding of structures from steel and aluminium sheets of 0.4–2.5 mm thickness using wire of 0.8–1.2 mm diameter [27]. The single-sided welding is performed without preliminary drilling of sheets in different spatial positions with a radius of service up to 15 m. Duration of welding one spot is 0.8–4.0 s, device mass with wire — 7 kg, power source — 3 kg. Steel structures are welded in CO_2, aluminium structures — in argon. Equipment is rational for arc spot welding of frameworks, bodies, cabins and hangars.

Company «Krompton Parkinson» used rivet welding in manufacture of kitchen utensils [28]. To weld on handles to the pots and pans, a specialized head «Kromp-arc», power source with a rectifier and specialized assembly device are used.

Over the recent years a specialized welding installation PSW-500 for plasma spot welding was developed in Germany [29]. From the statement of authors the installation has great advantages as compared with the equipment for the resistance spot and laser welding. They consist in the lower cost of equipment and feasibility of a single-sided access to product welded (for example, to the pipe or hollow body). The plasma torch is cooled by water. Filler wire is not fed to the zone of welding. Welding is performed at direct current (straight polarity).

The plasma arc melts the part by alternating pulses of current. Special focusing of plasma makes it possible to decrease the HAZ. The installation is suitable for welding carbon and alloyed steels, aluminium, copper and their alloys of up to 2.5 mm thickness. Welding can be performed manually, by automatic machines and robots. Variant of welding in argon with tungsten electrode with a conventional arc is possible.

The experiments showed that the arc with tungsten electrode can be applied for formation of 3–10 mm diameter holes in upper sheets of up to 3–5 mm thickness. Holes are burnt-through at currents up to 500 A. After the sheet burning-through the arc is disconnected temporary and the weld pool molten metal is blown out by a shielding gas jet. Gas jet smoothes the hole walls.

The larger thickness of the upper sheet can be melted out by a compressed plasma jet. In both cases electrode wire of 1.2–1.6 mm diameter is fed to the weld pool after the hole formation. At the end of the cycle the welding current and the wire feed speed are reduced to provide a good shape of rivet welds.

The least strength is characteristic of rivet welds made by the tungsten electrode in argon without use of the filler wire. A significant scatter of results of mechanical tests had also the joints with an increased gap between parts (above 0.2 mm). Stress concentration at the nugget edge leads to the formation of cold cracks that decrease the fatigue resistance of welded joints.

The arc spot welding is rational instead of a manual riveting, welding with intermittent and plug welds. Arc spot welding is most efficient in CO_2 or in mixture of Ar + CO_2 with a preliminary formation of holes at the upper plate using a plasma jet.

The further development of the arc spot welding method is associated with the use of a hybrid technology, including the plasma and arc welding with separate control of penetration of product and welding-up of crater. The most stable quality of welded joints can be attained at synergic control of condition parameters.

CONCLUSIONS

1. It was established that in arc spot consumable electrode welding in active gases (CO_2, Ar + CO_2) the quality overlap joints made from carbon and alloyed steels of up to 5 mm thickness are produced as a result of a through penetration of the upper sheet and subsequent its fusion with a lower element. In case of consumable and non-consumable electrode welding of aluminium, copper, titanium and alloys on their base the argon, helium or their mixtures are used as a shielding gas. If the thickness of metal welded is more than 5 mm, a hole, whose diameter exceeds the electrode wire diameter by 3–8 mm, is drilled in the upper sheet.

2. It is shown that the optimum parameters of single or double pulses in arc spot welding (welding current, arc voltage, electrode wire feed speed, time of welding) should be pre-programmed depending on grade and thickness of metal welded, diameter and composition of electrode wire, consumption and composition of the shielding gas. The rivet welds, made using electrode wire at minimum gaps between the elements welded (0.1–0.2 mm), possess the highest strength. To form the through holes in the upper and lower sheet the arc with a tungsten electrode, compressed by a plasma gas (for example, argon) can be used.

3. The final aim of the developments of combined and hybrid processes of arc spot welding is to widen the technological capabilities of consumable and non-consumable welding, to increase the efficiency of welding and to improve the quality of welded joints. The search for rational schemes of design of processes of spot plasma-arc welding and equipment for their realization should be connected with investigation of physical peculiarities of welding arcs, combined with plasma.

1. (1974) *Technology of electric fusion welding of metals and alloys*. Ed. by B.E. Paton. Moscow: Mashinostroenie.
2. Paton, B.E., Voropaj, N.M., Buchinsky, V.N. et al. (1977) Control of arc welding process by programming of electrode wire feed speed. *Avtomatich. Svarka*, **1**, 1–5, 15.
3. Voropaj, N.M. (1996) Parameters and technological features of arc welding with pulsed feed of electrode and filler wire. *Ibid.*, **10**, 3–9.
4. Killing, R. (1997) Das MAG — Mehrdrahtschweissen. *Praktiker*, **2**, 243–245.
5. Voropaj, N.M., Protsenko, P.P. (2000) Features of weld and HAZ formation in gas-shielded pulsed twin-arc welding

in high-strength low-alloyed steels. *The Paton Welding J.*, **8**, 40–46.
6. Voropaj, N.M., Ilyushenko, V.M., Lankin, Yu.N. (1999) Peculiarities of pulsed-arc welding with synergetic control of parameters. Review. *Avtomatich. Svarka*, **6**, 26–32.
7. Voropaj, N.M., Ilyushenko, V.M. (2003) Hybrid processes of arc and plasma welding. *Svarshchik*, **2**, 22–27.
8. Vajnbojm, D.I. (1966) *Automatic arc spot welding*. Moscow-Leningrad: Mashinostroenie.
9. *GOST 14776–80*. Arc welding. Spot welded joints. General types, structural elements and sizes. Introd. 01.01.80.
10. Novozhilov, N.M., Sokolova, A.M. (1956) CO_2 rivet welding. *Svarochn. Proizvodstvo*, **7**, 10–13.
11. Potapievsky, A.G., Porubinovsky, A.I. (1957) CO_2 rivet welding of sheet metal. *Avtomatich. Svarka*, **6**, 99–102.
12. Tereshchenko, V.I., Sharovolsky, A.N., Sidorenko, K.A. et al. (1983) Features of CO_2 arc spot consumable-electrode welding. *Ibid.*, **9**, 51–53.
13. Tatarinov, V.S., Tereshchenko, V.M., Iorsh, E.T. et al. (1986) Corrosion fatigue resistance of overlap joints produced by arc spot welding. *Ibid.*, **7**, 46–48.
14. Rosenkranz, H., Kiese, S. (1972) Punktschweissen unter Schutzgas. *ZIS-Mitt.*, **3**, 348–353.
15. Brodsky, A.Ya. (1958) New method of penetration rivet welding. *Svarochn. Proizvodstvo*, **10**, 18–21.
16. Vinogradov, V.S. (1964) Peculiarities of rivet welded joints of aluminium alloys. *Ibid.*, **6**, 28–31.
17. Geridoenmez, O. (1969) Schutzgaspunktschweissen der hochfesten Aluminiumlegierung Al–Zn–Mg. *Schweissen und Schneiden*, **2**, 64–70.
18. Kehoe, I.W., Bichsel, H.I. (1956) Inert-gas-shielded metal-arc spot process. *Welding J.*, **9**, 895–903.
19. Dovbishchenko, I.V., Mashin, V.S., Shonin, V.A. et al. (2003) Properties of overlap joints of aluminium alloys produced by spot arc welding. *The Paton Welding J.*, **1**, 6–11.
20. Steer, I.L., Copleston, F.W. (1957) Developments in the argon-arc spot welding process. *Welding and Metal Fabr.*, **8**, 282–288.
21. Clean, M. (1955) Inert-gas-shielded tungsten-arc spot welding. *Welding J.*, **7**, 648–656.
22. Lozovsky, V.P., Timoshenko, A.N. (1987) Arc spot welding of thin sheet overlap aluminium alloy joints. *Avtomatich. Svarka*, **7**, 49–51.
23. Timoshenko, A.N., Lozovsky, V.P., Novikov, V.I. (1977) Helium-shielded non-consumable electrode arc spot welding of aluminium alloys. *Ibid.*, **7**, 69–71.
24. Timoshenko, A.N. (2003) Immersed-arc spot welding of aluminium alloys. In: *Proc. of Int. Conf. on Current Problems in Welding and Life of Structures*, Kiev, Nov. 24–26, 2003. Kiev: PWI.
25. Tarasov, N.M., Kapustin, S.S. (2001) Arc spot welding of aluminium alloy thin-sheet elements using a drop dosing of electrode metal. *The Paton Welding J.*, **7**, 24–26.
26. Kulikov, F.R., Bulina, A.I., Frolov, N.G. (1964) Mechanised argon-arc spot welding of stainless steel SN-2 and titanium alloy OT-4. *Svarochn. Proizvodstvo*, **4**, 16–19.
27. Zyakhor, V.K. (1998) Unit for arc spot welding of sheet structures of A1830 type. *Avtomatich. Svarka*, **3**, 55.
28. (1969) Stud welding — a method of speeding up production. *Light Prod. Eng.*, **4**, 23.
29. (2003) Plasma-Punktschweissen mit dem Plasma Spot Welder. *Schweissen und Schneiden*, **5**, 224–225.

USE OF WEB-TECHNOLOGIES TO IMPROVE THE COMPETITIVENESS OF UKRAINIAN ENGINEERING PLANTS

V.S. KOVALENKO and **V.V. KOLPAKOV**
Laser Technology Institute at NTUU «Kiev Polytechnic Institute»

Technical solutions intended to increase the competitiveness of engineering plants through reduction of the production time, centralization of manufacturing and distribution of orders using web-technologies have been identified. Main principles of development of a web-site as an acceptor of orders have been considered, and versions of software implementation of a central server and acceptable versions of transfer, reception and performance of a product manufacturing order have been analyzed by considering the example of the server of the Laser Technology Institute of the National Technical University of Ukraine «Kiev Polytechnic Institute». The need to promptly set up a centralized web-structure to control orders of small and medium-sized engineering plants of Ukraine for raising their foreign competitiveness is proved.

Keywords: *mechanical engineering, automation, laser processing of materials, Internet, web-technologies, XML, AutoCAD, electronic commerce, network diagram*

Change of the global management structure, principles of management and interaction of plants of the engineering industry of Ukraine over the last decade led to emergence of small and medium-sized plants, competing with each other in the inner market. Their emergence is due to disintegration of centralized management and disappearance of government contracts for engineering products. The plants were left to their own resources, and the newly established borders of independent states have turned the former state cooperation of the plants into a historic nonsense. In the period of globalization of world economy dissociation of gigantic engineering plants and almost complete discontinuation of centralized funding affected Ukraine's position in the world rating of developed countries. Actually all the leading mechanical engineering industries ceased to be competitive.

Continuous efforts of a number of plants to preserve foreign trade orders and obtain new ones can be regarded as a definite asset. Timely reorientation of part of the plants in shipbuilding and aircraft construction to meet the demands of the word market and comply with the continuing orders for replacement of worn components in the already sold equipment saved a significant number of engineering plants from ruin. Nonetheless, any kind of leadership of local industry in the world economy is out of the question.

Problem. Under globalization of the economy one of the decisive factors for plant competitiveness is their ability to integrate into a new system of obtaining orders, maximum shortening of the turnaround time and lowering the cost of a unit of product [1]. Small and medium-sized plants left on their own usually fulfill small and medium-size batch orders. Obvious principles of lowering of the cost due to increase of output of one product type are not applicable to them. Considering a certain lagging behind in the technological sphere of design and introduction of new local products, which has been observed lately, plants survival is based on manufacturing components for old equipment and single orders. Absence of a centralized structure of establishing and external acceptance of a possible flow of foreign orders makes it impossible for separated Ukrainian manufacturers of engineering products to reach external market as one industrial complex [2].

Review of existing solutions. The greatest effect in acceleration of the manufacturing process cycle is provided by information technologies in standardization, unification and electronic classification of the fixtures, equipment and finished products. Electronic bases of unified products, list of manufacturers and accessibility of electronic payments allowed establishing electronic commerce sites based on organizing web-service and centralizing product manufacturing.

The main directions of introduction of the developments and promising research are

- web-sites of order acceptors;
- data bases of accessible production facilities;
- consultative data bases for selection of the fixtures and material for manufacturing the specified product type;
- organizing closed-loop virtual production.

Web-systematizing and data base to generate recommendations for selection of the cutting tools depending on product material [3, 4] operates in the server of the University of Kon-Ku (Korea). A model has been developed and elements of web-interfacing of design documentation, unification and operation of plants of Stuttgart industrial complex have been introduced in the server of Stuttgart Institute of Industrial Development and Manufacturing (Germany). Ministry of Science and Industry of the Korean People's Republic has recently started funding research on standardization and establishing a website of remote design of hydraulic systems and pumping units [5].

Initial purpose of information technologies of reducing the time and cost of document circulation in an individual plant has developed into a fundamentally new stage of collective solution of engineering

© V.S. KOVALENKO and V.V. KOLPAKOV, 2004

problems of design, manufacturing and sale of products. The discussed problem of centralizing and improving the competitiveness of plants of the engineering complex of Ukraine has been solved to some degree in the structure of transnational automotive giant monopolies by unification of parts and manufacturing the components of a common car prototype, using the principle of international division of labour, web-technologies of design and distribution of orders in the local spatially dispersed production facilities.

Unfortunately, web-services provided by local servers to Ukrainian plants are reduced to trivial advertising information about the plant existence, its address, list of the «products that can be manufactured».

Problem definition. A real path to the fastest breakthrough in the engineering industry of Ukraine to reach the external market using the existing potential is development of a market-oriented, but centralized and fast system of support in securing orders for small- and medium-sized plants, based on web-technology of processing, analysis and transfer of the data. Such a technology is currently being developed by a number of Western corporations [3–6], and it essentially is the main administrative tendency to improve the manufacturing efficiency [1, 2]. In practice the considered approach means partial reanimation of the idea of a centralized industry, but in an electronic format, foreign economy oriented and independent of government bodies. Implementation of the system is based on interfacing data bases of product characteristics, network analysis of the load on process equipment in a specific plant, its production capacity and additional aspects of order fulfillment. This actually is an insignificant, but meaningful correction of the tendencies of developments of Western giant engineering corporations in terms of network management of the resources and use of the so-called globalization within an individual country. In the proposed version of export potential reanimation the Ukrainian engineering industry will have the role of a major industrial corporation of Western type with spatially dispersed and independent affiliated branches. Unlike the regular projects of support and development of small- and medium-sized plants, it is intended to increase the competitiveness of such plants by fast processing of all possible orders and widening the product range, using an «external order acceptor», providing their increased competitiveness and not detracting from their independence in selecting their development strategy. As a result, not a single plant with limited capacity, but an entire industry with the complete capacity range and possible product range enters the international market. In technical terms the central web-site can have the role of external accumulator of orders for manufacturing the products of local plants. This site should use as the basis the data base with XML-marking, which will permit interfacing the software of the main customers and manufacturers from the engineering industry in the Internet without creating intermediate archivated files of technical documentation [7]. Site activation for «acceptance» and transfer of product prototypes for direct manufacturing to a Ukrainian plant via the Internet enables increasing the competitiveness of the local manufacturing, fitted with laser systems, against Western plants fitted with the same equipment, but having, through obvious reasons, a higher product cost.

Technical solutions for construction of the software to ensure order acceptance. *Main elements of the software for the order acceptor web-site.* Principles and methods of programming the electronic business plants are filled with new capabilities avalanche-like. The main technical solutions for creation of an external Internet-acceptor of orders have been defined in the general case. A typical web-site for electronic processing of orders includes the following program modules (Figure 1) [8]:

- presentation of general information in the form of HTML-files with possible inclusion of active advertising pages («saved scenarios»);
- formation and processing of the data base of orders with active acceptance modules;
- information about the customer («common data base»);
- formation and processing of a data file from / for the data base of orders, using active modules of acceptance of information on the characteristics of the product suggested for manufacturing («mechanism of data base processing»);
- processing the file of order payment and issuing a command for manufacturing and release of goods («mechanism of active server applications»);
- support and recording of receiving of the order by the user («mechanism of data processing»).

During construction of a virtual manufacturing the last listed items should be complemented by:

- evaluation of accessibility of equipment, which enables fulfilling the order and calculation of the possible manufacturing time;
- preparation of technical documentation for manufacturing and transfer for performance.

Principles of coordination of data bases and graphic documentation in the Internet. Web-sites can

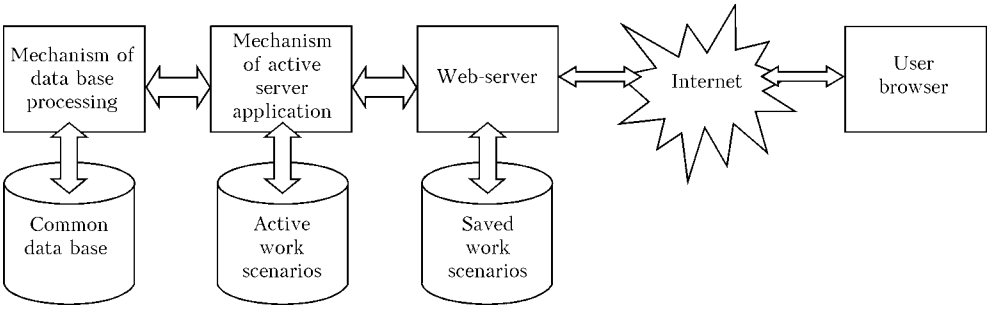

Figure 1. Schematic of implementation of a web-site of order acceptor

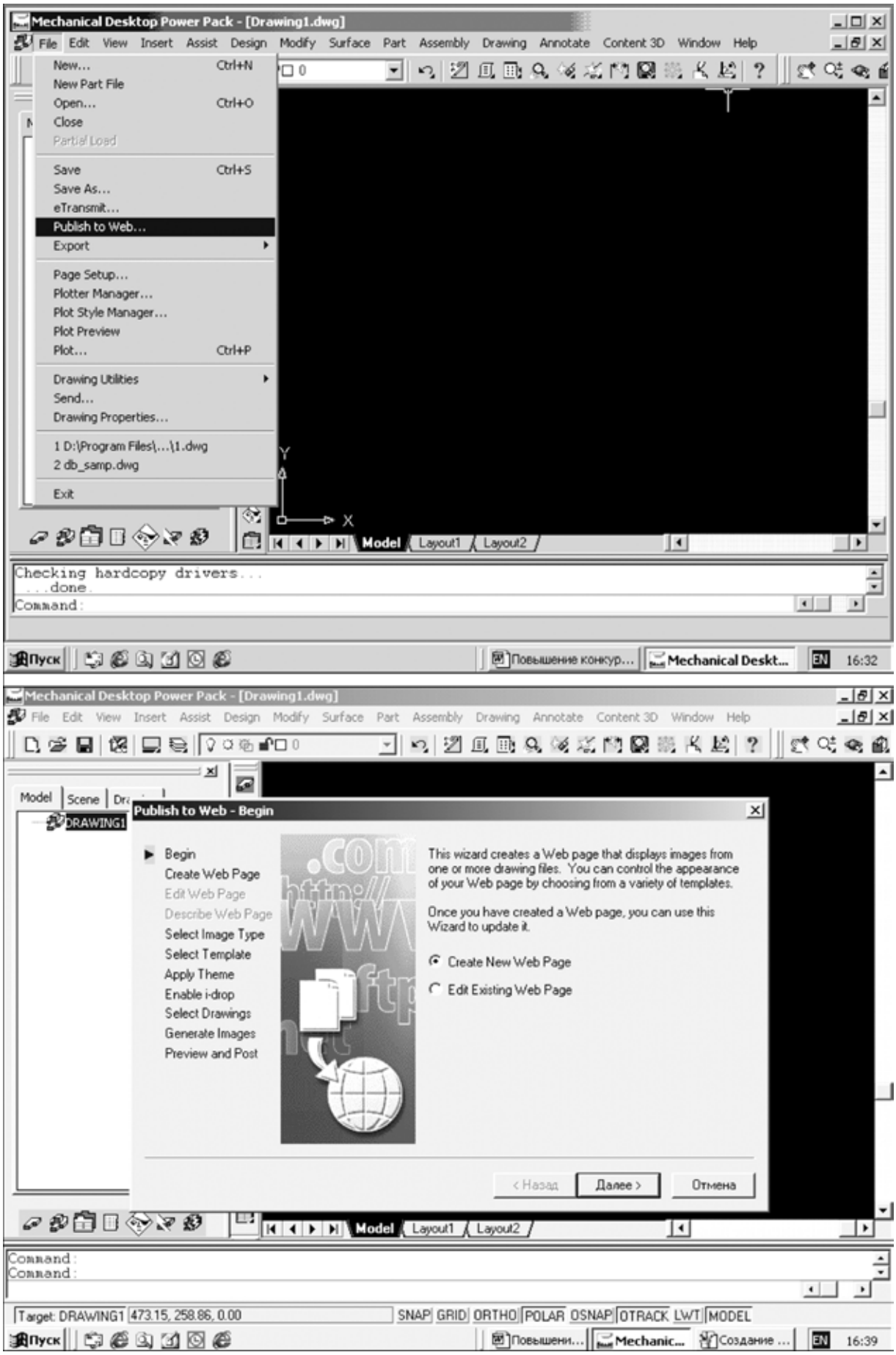

Figure 2. Sequential windows of forming a web-page in DWF format in AutoCAD 2002 environment

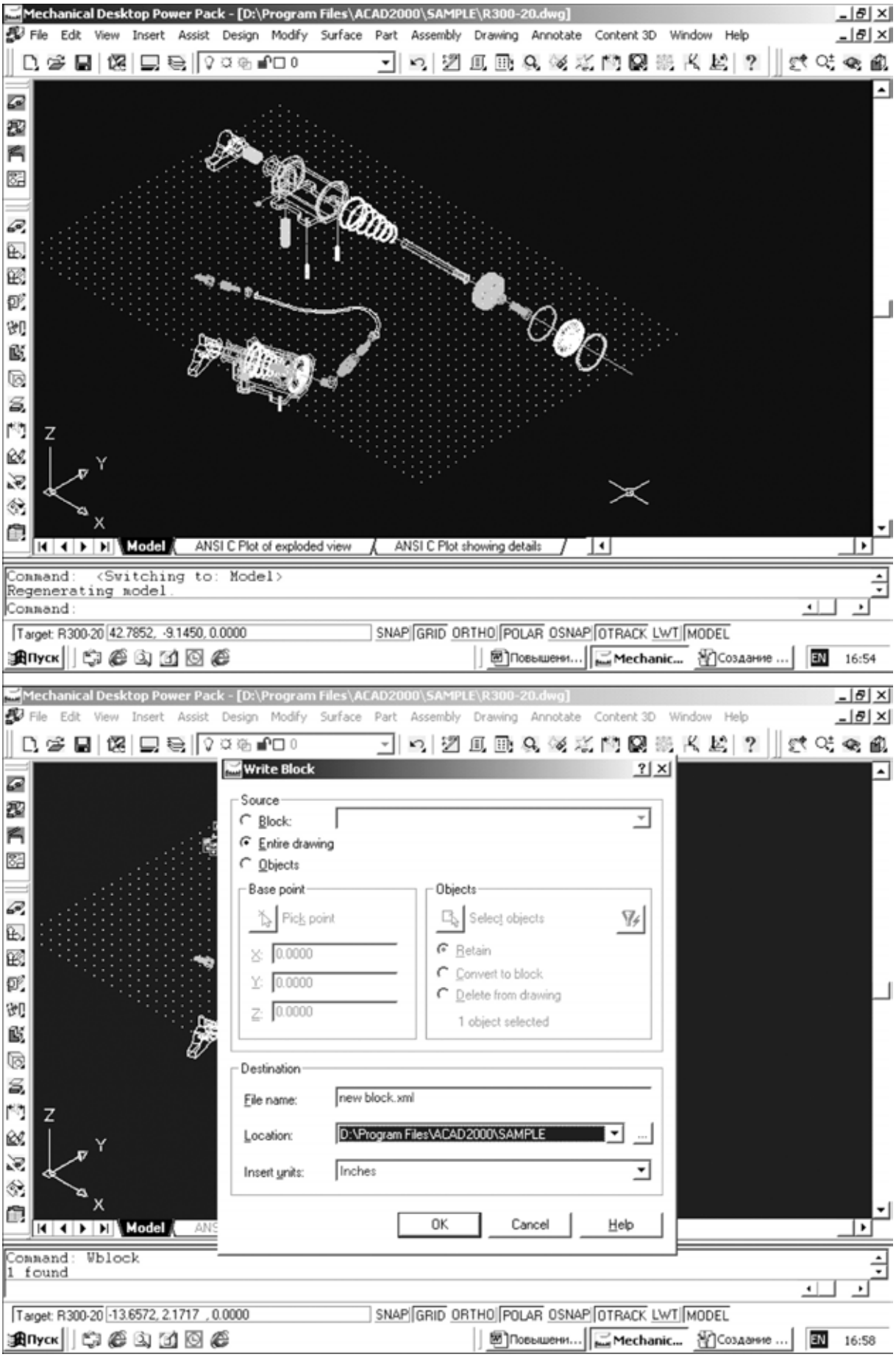

Figure 3. Sequence of generation of XML-file of a blank in AutoCAD 2002

Program product	*Cost, USD**
Microsoft Windows NT-server	400–900
Microsoft SQL-server	1000–1200
ASP	800–1400
Java	300–350
AutoCAD 2002 / 2004	5300–5590

*Data are given by materials of «HotLine» journal.

transfer various types of graphic information for processing to the user. The most widely accepted are JPEG, GIF, PNG and BMP formats. Unfortunately, the basic formats of CAD systems for mechanical engineering products cannot be used for presentation in the web-site, because of different data communications protocols, principles of structure formation and data archiving. It should be taken into account that the above Internet-formats are raster ones and lose the image quality at scaling, do not accommodate command performance of graphic constructions and, therefore, are unacceptable for providing step-by-step execution of geometrical elements by a PNC machine tool. The main current CAD formats are DWG, DXF and DWF. A figure compatible with www and simultaneously preserving the specifics of transferring the drawing to a plotter or PNC board can be created in DWF-format specially developed for inclusion into a web-page or another text document. Use of a DWF-file to place and fulfill an order requires each user to have not only an additional program module of file exchange, I-drop, disseminated by AutoDesk free of charge, but also a copy of the main AutoCAD program module of this company [9]. Figure 2 gives the sequence of windows for generating a file in DWF format in AutoCAD 2002 environment.

Automated functions of file layout on a web-page were a new feature of AutoCAD 2002 product and in addition to MeetNow functions, providing joint viewing and editing of documentation in the local network, they became a significant element in the tendencies of joint developed of the CAD and Internet systems.

The most promising software base for setting up a web-acceptor of orders for the mechanical engineering industry can be the intensively developing areas of design software for CAD systems, principles of web-support of access to common resources and capabilities of forming generalized data bases in the format of extensible markup language XML [6]. World producers of the software have mastered commercial release of XML-interfacing of data bases and presentation of web-browsers in 2000–2002. AutoDesk Company has also commercially introduced DesignXML-module as a standard extension for generating an XML-file of the designed item in AutoCAD 2002.

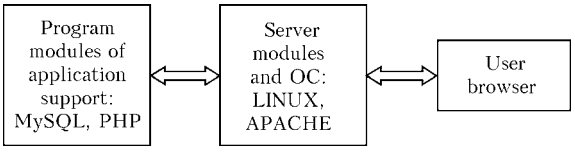

Figure 4. General schematic of data communication between the server and user in the case of using program products with an open code

XML-file of the part designed and transferred for manufacturing can be generated in this most powerful CAD software product, isolating the structure object saved in the file and forcedly replacing standard extension .dwg by .xml (Figure 3). This will result in a file structured for XML-marking and acceptable for presentation in the Internet.

In view of the above-said, selection of XML-programming as a basis for special software in implementation of a web-acceptor and distributor of orders is practically obvious.

Selection of software and operating system for implementation of a web-site. *Solution of the problem of using license software and certification of electronic business programs*. A large number of publications on electronic commerce of Western market are helping the advertising campaign of the actual field of electronic sales and specialized self-advertisement of the authors. In addition, these publications are designed for financially secure businesses, purchasing Microsoft license programs, thus advertising the products of this company. As a rule in Western publications Microsoft Windows NT-server is selected as the server operating environment, IIS as the mechanism of server function support, ASP as the basic environment for programming server applications, and Microsoft SQL-server of various modifications as the environment for forming the data base. Java (producer is SUN company) and JavaScript (Microsoft) are the most often mentioned language environments for activation of the applications.

Average cost of the installation of the above license programs is given in the Table. Considering the need for programmers working on specialized programs and server operation support, the cost of the work will add up to a considerable sum for a government organization, small business or unit of an educational establishment. Use of unlicensed software by the authors to create commercial extensions is regarded as unacceptable and is not considered.

Open-code programs, namely LINUX and FreeBSD (among operating systems), APACHE (among server programs), PHP (in the field of language structures of dynamic programming of web-pages) and MySQL (in the field of data base construction) have become an acceptable alternative to software products of Microsoft class. Openness of the initial program code, ability to use them without licensing and low cost of these software products determined their wide acceptance and popularity with the Internet providers and qualified programmers, developing specialized web-applications. The general schematic of data communication between the server and user in the case of using software products with an open code is given in Figure 4.

Most of the providers offer disc space for placing active user servers, applying exactly this software. A disadvantage of selecting open-code programs to implement server applications of electronic commerce are high requirements to the qualifications of the programmer managing the web-project. However, due to a number of historically formed conditions, availabil-

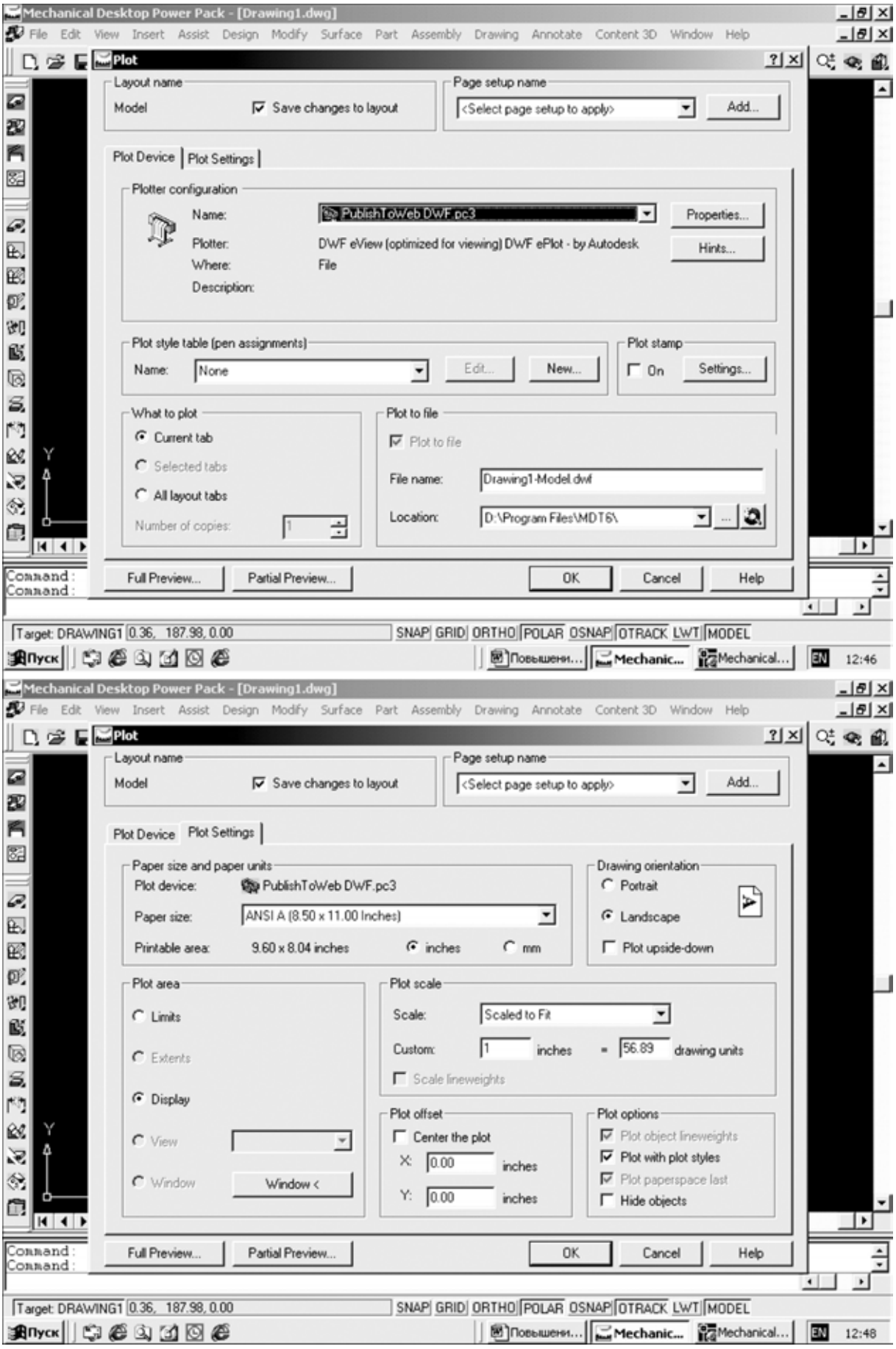

Figure 5. Principles of execution of commands for transfer of the drawing to the plotter in the structure of Mechanical DeskTop 6.0 software

ity of qualified programmers is an advantage of the Ukrainian labour-market.

Technical solutions of the problem of selection of the method of making the finished product and potential manufacturer. The most complete description of modern formalizing of the problem of making the finished product and searching for a potential manufacturer in the structure of virtual plants, as well as its solution are given in the papers on «Information Management and Integration of Manufacturing Processes» of the Proceedings of 35th International Seminar of CIRP on «Manufacturing Technologies in the Information Age» [10]. The main principles for solving this problem are based on the time profiles of product manufacturing and methods of network planning of the machine fleet usage, complemented by modern methods of data processing and transfer.

Technical solutions of transfer of the program task of making the product for execution by the laser unit. Technical solutions of machine control in keeping with the set program code were identified simultaneously with introduction of PNC machines. Their operation is based on the principles of execution of the command-by-command code of the selected programming language environment.

Ukraine lagging behind in manufacturing of machines and high-technology equipment observed over the last years, was only slightly compensated by purchasing of foreign machines on state credits or under projects of technical assistance. It should be noted that practically all the Western machines have automatic control systems. The most advanced metalworking equipment in the Ukrainian market are laser systems for steel cutting, mechanical machines for metal severing ---- presses and benders of BYSTRONIC, Switzerland, and AMADA, Japan.

Practically all the laser systems of these companies are fitted with PNC with programs of calculation of optimum cutting of a sheet, as well as program-oriented system of controlling the characteristics and motion of the cutting beam or displacement of the process table. A trivial solution of transfer of the program task for execution by the laser beam can be compared with drawing output to a plotter. This problem has been comprehensively developed and does not require any significant additional engineering solutions, except for, probably, finding a driver for interfacing the technical devices of the used computer machinery and the laser system. The principles of solving the problem in the structure of Mechanical DeskTop 6.0 software (manufactured by AutoDesk) are shown in Figure 5.

In a similar, although a somewhat more complicated fashion, is the numeric program processing performed for the operations of drilling, milling, turning and other processes of material processing, not always related to laser technology, but taking up a rather large volume of work in manufacturing of mechanical engineering products.

The problem of transfer of the program task of laser system operation appears to be much more complicated when fulfilling the functions of part strengthening or making the product by the principle of laser sintering of powder mass [1]. In this case one cannot do without development of unique software or use of additional license program modules.

Description of the principles of construction of the software for control of such processes is beyond the scope of material considered in this paper.

In any case, technical solutions of transfer of program task of product formation for performance of laser processing operation cannot become a stumbling block in the path of solving the problem of centralizing and increasing the competitiveness of the products of engineering plants of Ukraine.

CONCLUSIONS

1. Use of Internet technology for centralizing obtaining of export orders, as well as their analysis, processing and optimum distribution in the small and medium-sized businesses of the engineering complex of Ukraine is a real path for a significant increase of the competitiveness of the industry and reducing the small-batch shadow manufacturing.

2. The main order acceptor can be a web-site, using the capabilities of conversion and XML-presentation of technical documentation for product manufacturing, data base of plants interested in getting the order, characteristics of their engineering facilities and load schedule.

3. Order forming and its transfer for manufacturing can be performed both directly through XML-file of the central web-site, and using a file of an electronic drawing of the part, acceptable for output to the machine plotter.

4. The plan of plant work load should be made by a program module of network planning, with criterial selection of the next load site by price, speed and quality estimates.

1. Kovalenko, V.S. (2002) Mechanical engineering in the new millenium: from processing of billet to growth of finished part. In: *Abstr. of pap. of 2nd Intermed. Int. Sci.-Techn. Conf. on Efficiency of Realisation of Scientific, Resource and Industrial Potential in Current Conditions*, Slavskoe, 25 Febr.–1 March, 2002. Kiev: Nauka, Tekhnika i Tekhnologiya.
2. Kovalenko, V.S., Kolpakov, V.V. (2004) Engineering solutions of increase of competitiveness of small and middle-sized mechanical engineering plans using the web-technologies. In: *Abstr. of pap. of 4th Intermed. Int. Sci.-Techn. Conf. on Efficiency of Realisation of Scientific, Resource and Industrial Potential in Current Conditions*, Slavskoe, Febr. 2–7, 2004. Kiev: Nauka, Tekhnika i Tekhnologiya.
3. McMains, S., Sequin, C., Smith, C. et al. (1999–2000) Internet-based design and manufacturing computer science department and mechanical engineering departments of University of California, Berkeley. *Final Report 1999–2000 for MICRO project 99-106.*
4. Smith, C. (1999) *The manufacturing advisory service: Web-based process and material selection*, Ph. D. Thesis of U.C. Berkeley Mechanical Eng. Depart.
5. McMains, S., Sequin, C., Smith, C. (1999) SIF: A solids interchange format for rapid prototyping. *Techn. Paper PE99-117, Society of Man. Eng.* Dearborn.
6. Kim, J.H., Wang, F.C., Sequin, C. et al. (1999) Design for machining over internet. In: *Proc. of Design Engineering Techn. Conf. on Computer Integrated Engineering Paper No. DETC'99/CIE-9082*, Las Vegas, Sept. 1999.
7. Spenser, P. (2001) *XML. Design and realisation*. Moscow: Lori.
8. Frizell, S.A. (2001) Pattern-based design methodology for web-based instruction department of computer science and software engineering of Auburn University. *Res. sum. 09.2001*.
9. Omura, D. (2002) *AutoCAD 2002*. Moscow: Lori.
10. (2002) Manufacturing technology in the information age. In: *Proc. of 35th CIRP Int. Seminar on Manufacturing Systems*, Seoul, May 13–15, 2002.

EVALUATION OF MECHANICAL STRENGTH OF A WELDED PIEZOTRANSDUCER

Yu.G. ZADOROZHNY and **M.I. ZORIN**
OJSC «Predpriyatie SENSOR», Chernigov, Ukraine

A procedure is proposed for evaluation of mechanical strength of welded metal-piezoceramic bimorph by the size of fracture surface in peizoceramics. Dependencies of the strength of a welded metal-piezoceramic structure on welding modes are given. A welding mode is established, providing the required level of welded structure quality.

Keywords: *diffusion bonding, bimorph, piezoceramics, welded structure, strength*

Accelerometers using peizoceramics have become widely accepted in measuring systems. Their application is due to a stable quality of products and a wide range of service characteristics. Known are the designs of piezoaccelerometers and piezoengines, using piezoceramic bimorhps as transducers [1]. The latter are mainly made by adhesion bonding. Presence of an elastic adhesive interlayer in them leads to piezoelectric characteristics, unstable in time or at temperature variations, this limiting the working range of bimorph temperature and their operating life. In addition, mechanical strength of the adhesion bond is much lower than that of piezoceramics (least strong element of the structure). This does not permit using them in structures with higher mechanical loads.

The goal of the work consisted in development of a procedure for evaluation of mechanical strength of the metal-ceramic bimorph and determination of the mode of diffusion bonding, providing maximum strength of the weldment.

Bimorph design (Figure 1) includes two piezoelements of TsTS-19 piezoceramics connected to each other via a metal electrode of VT-6 titanium 0.2 mm thick. Metal plates of the bimorph are made of titanium foil of the same thickness. Polarization of piezoelements can be provided in the same direction or in opposition.

Mechanical strength of a metal-piezoceramic structure mainly depends on the strength of the transition zone of the welded joint (weld) and level of mechanical stresses in a welded structure. The transition zone can have a high strength, which can be even higher than that of one of the materials being welded. However, it will be minimum at a considerable level of mechanical stresses in a weldment. When conducting measurements of the strength of a weldment in tear, shear and bending, it is necessary to take into account the influence of the structure on it [2, 3]. In practice mechanical strength is evaluated on mock-ups, having dimensions close to those of the real structure.

During diffusion bonding improvement of mechanical strength of a weld is accompanied by a change in the nature of material fracture [4]. At a low strength the fracture proceeds over the surface of material contact, and with its increase through the transition zone. Further increase in strength is accompanied by fracture running through the piezoceramics. Thus, the nature of surface fracture of a welded joint through the piezoceramics or the zone of contact of materials is indicative of the strength in each point in the plane of initial contact of materials, this allowing quantitative evaluation of weldments strength to be performed by the area of fracture surface in the zone of initial contact of materials.

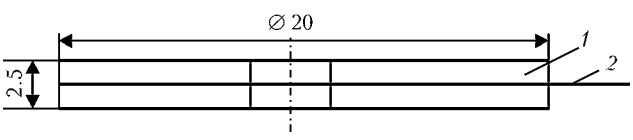

Figure 1. Schematic of a metal-ceramic bimorph: *1* — piezoceramics; *2* — titanium electrode

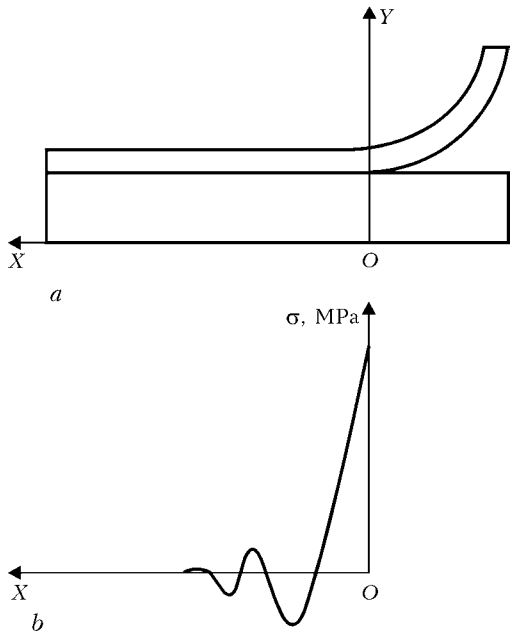

Figure 2. Schematic of fracture of a laminated structure (*a*) and distribution of normal stresses on the metal–piezoceramic interface (*b*): *O* — point of the start of delamination

© Yu.G. ZADOROZHNY and M.I. ZORIN, 2004

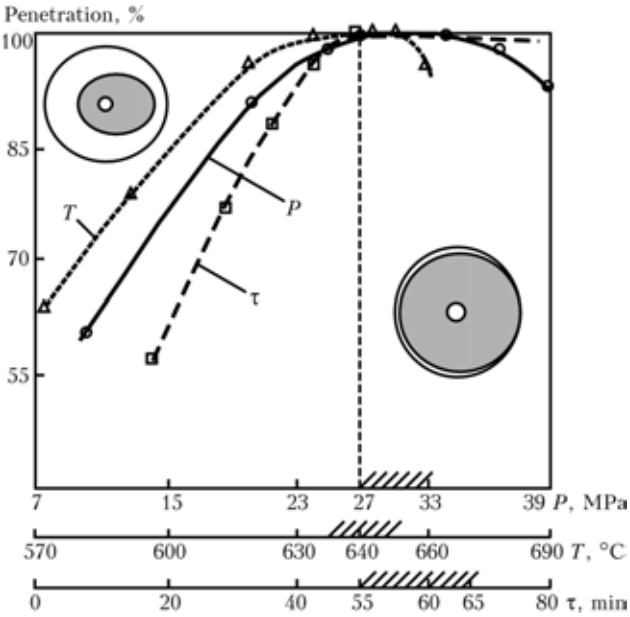

Figure 3. Dependence of the fracture surface of a welded joint through piezoceramics on the welding mode: P — compression force; T –·– welding temperature; τ — welding time

A delamination method [5] is used for breaking up the metal-ceramic laminated structure. With this method, the force is applied to a flexible metal electrode and maximum breaking stresses in a welded structure are implemented in the transition zone of the welded joint (Figure 2).

Area of the surface of fracture of a weld through the piezoceramics is directly proportional to the welded structure strength. This dependence was used for establishing a welding mode, providing maximum strength of the welded structure of the bimorph.

Influence of the parameters of diffusion bonding process on the mechanical strength of the bimorph was studied in the mode of a single-factor experiment. The data of [2, 6] was the basis to establish the mode, providing a penetration close to the maximum penetration over the entire surface of the initial contact of materials. One or several parameters of the mode were changed to determine their influence on the area of fracture surface of a welded joint in the piezoceramics. All the products were prepared with the same flatness and ceramics from one batch was used. The process was conducted at residual pressured of the gas in the chamber below 0.01 Pa.

Evaluation of the obtained dependencies (Figure 3) shows that the joint strength (area of fracture surface in the piezoceramics) rises with increase of welding mode parameters and has maximum values in a certain range. Further increase of the values of welding mode parameters is accompanied by fracture of the piezoceramic part.

A piezoelectric bimorph structure is used as a sensitive element in vibropacks of VPE type, designed for measurement of the parameters of vibration in power units of thermal and nuclear power plants. Ranges of welding mode parameters, providing the maximum strength of the welded structure (T = 640–650 °C, P = 27–33 MPa, τ = 55–65 min) were also established.

1. Glozman, I.A. (1972) *Piezoceramics*. Moscow: Energiya.
2. Metelkin, I.I., Pavlova, M.A., Pozdeeva, N.V. (1977) *Welding of ceramics to metal*. Moscow: Metallurgiya.
3. Musin, R.A., Konyushkov, G.V. (1991) *Joining of metals to ceramics*. Moscow: Mashinostroenie.
4. Zadorozhny, Yu.G. (2003) Mechanical strength of welded structure from high-temperature piezoceramics and structural alloy. *Svarshchik*, **3**, 38–39.
5. Uglov, A.A., Anishchenko, L.M., Kuznetsov, S.E. (1987) *Adhesive strength of films*. Moscow: Radio i Zvyaz.
6. Zadorozhny, Yu.G., Bachin, V.A. (1986) *Diffusion bonding of glass and ceramics to metals*. Moscow: Mashinostroenie.